


 Cite this: *RSC Adv.*, 2026, **16**, 3349

## Design, synthesis, *in silico* studies, and antiproliferative activity of a novel series of thiazole/1,2,3-triazole hybrids as apoptosis inducers and multi-kinase inhibitors endowed with anti-breast cancer activity

Fatma A. M. Mohamed,<sup>\*a</sup> Saleha Y. M. Alakilli,<sup>b</sup> Hassan H. Alhassan,<sup>c</sup> Sara Osman Yousif,<sup>a</sup> Eid Alatwi,<sup>d</sup> Hesham A. M. Gomaa,<sup>d</sup> Heba Abu Alruba,<sup>a</sup> Bandar A. Alyami,<sup>e</sup> Ahmed H. Abdelhafez,<sup>f</sup> Stefan Bräse<sup>g</sup> and Bahaa G. M. Youssif<sup>h</sup>

A novel series of thiazole/1,2,3-triazole hybrids has been developed and evaluated for their *in vitro* anticancer efficacy. Compounds **10c**, **10e**, **10k**, **10m**, **10n**, and **10o** exhibited superior anticancer efficacy against the evaluated cancer cell lines, demonstrating a favorable safety profile, particularly against MCF-7 breast cancer, compared to erlotinib. The *in vitro* anti-breast cancer assay of compounds **10e** and **10k** demonstrated potent antiproliferative activity against the MCF-7 breast cancer cell line, with  $IC_{50}$  values of 24 nM and 21 nM, respectively, relative to the reference erlotinib, which exhibited an  $IC_{50}$  value of 40 nM. To elucidate their antiproliferative mechanism, tests for EGFR, HER-2, VEGFR-2, and BRAF<sup>V600E</sup> kinases were performed. Compounds **10e** and **10k** exhibited the highest potency as multi-EGFR/HER-2/VEGFR-2 kinase inhibitors, with  $IC_{50}$  values of  $73 \pm 4$  nM (EGFR),  $31 \pm 2$  nM (HER-2), and  $20 \pm 1$  nM (VEGFR-2), and  $69 \pm 4$  nM (EGFR),  $29 \pm 1$  nM (HER-2), and  $21 \pm 1$  nM (VEGFR-2), respectively. The BRAF<sup>V600E</sup> inhibitory testing results indicated weak to moderate effectiveness for the evaluated compounds. Findings from assays of apoptotic markers (Bax, Bcl2, and p53) indicate that apoptosis may contribute to the antiproliferative effects of the examined compounds. Analysis revealed that the 1,2,3-triazole moiety, the *para*-substituted methoxy group, and the chalcone moiety are essential variables in enhancing activity. The *in silico* docking studies against EGFR, HER-2, and VEGFR-2 revealed the importance of the phenyl 1,2,3-triazole moiety and the chalcone side chain in anticancer activity. The most potent compounds demonstrated drug-like properties and could serve as prototypes for future optimization. Compounds **10e** and **10k** may serve as examples of multi-targeting anticancer agents that function by blocking the EGFR, HER-2, and VEGFR-2 kinases.

Received 4th October 2025  
 Accepted 3rd January 2026

DOI: 10.1039/d5ra07556d  
[rsc.li/rsc-advances](http://rsc.li/rsc-advances)

### 1. Introduction

Cancer is characterized as a group of disorders that infiltrate other regions of the body.<sup>1</sup> Cancer is the second biggest cause of global mortality, following cardiac diseases, and constitutes a significant health burden.<sup>2-4</sup> Despite the availability of numerous effective anticancer therapies, their side effects, such as drug resistance, a lack of differentiation between malignant and benign cells, limitations of radiotherapy, and the need for surgical intervention, highlight the need for effective alternatives that employ a variety of mechanisms to achieve success.<sup>5-7</sup>

Protein tyrosine kinases (PTKs) serve a key role in human cell signaling, directing cellular proliferation, differentiation, angiogenesis, and many regulatory processes.<sup>8,9</sup> The over-expression of PTKs is essential in the genesis and progression of cancer due to their significant roles in cellular hemostasis.<sup>10</sup>

<sup>a</sup>Department of Clinical Laboratory Sciences, College of Applied Medical Sciences at Al-Qurayyat, Jouf University, Al-Qurayyat 77454, Saudi Arabia. E-mail: fatmaahmed@ju.edu.sa

<sup>b</sup>Department of Biological Sciences, Faculty of Sciences, King Abdulaziz University, Jeddah 23761, Saudi Arabia

<sup>c</sup>Department of Clinical Laboratories Sciences, College of Applied Medical Sciences, Jouf University, Sakaka 72388, Saudi Arabia

<sup>d</sup>Department of Pharmacology, College of Pharmacy, Jouf University, Sakaka 72388, Saudi Arabia

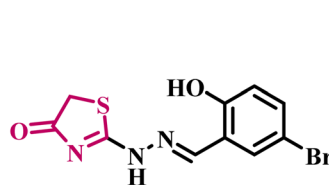
<sup>e</sup>Department of Pharmaceutical Chemistry, College of Pharmacy, Najran University, Najran, Saudi Arabia

<sup>f</sup>PharmaHelp Foundation Inc., Falls Church, Virginia, USA

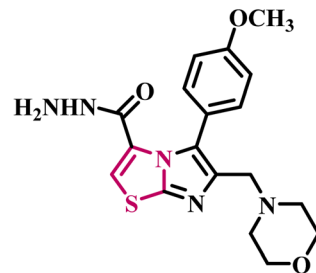
<sup>g</sup>Institute of Biological and Chemical Systems, IBCS-FMS, Karlsruhe Institute of Technology, 76131, Karlsruhe, Germany. E-mail: braese@kit.edu

<sup>h</sup>Department of Pharmaceutical Organic Chemistry, Faculty of Pharmacy, Assiut University, Assiut-71526, Egypt. E-mail: bgyoussif2@gmail.com; Tel: +201044353895





Compound I



Compound II

Fig. 1 Structures of thiazole derivatives I and II as dual EGFR/HER-2 inhibitors.

Moreover, PTK malfunction is fundamental to most cancer types, with PTKs constituting over 60% of all oncoproteins and proto-oncoproteins, which are pivotal in cancer pathology.<sup>11</sup> Epidermal growth factor receptor (EGFR or ErbB1) and human epidermal growth factor receptor 2 (HER-2 or ErbB2) are two PTKs within the Erb-B family, which are overexpressed in a variety of solid tumors, including colon, breast, ovarian, lung, and prostate cancers.<sup>12,13</sup> As a result, both receptors have been identified as plausible targets for cancer therapy.<sup>14,15</sup> Vascular endothelial growth factor receptor-2 (VEGFR-2)<sup>16</sup> is another crucial PTK that plays a role in angiogenesis, the process of producing new blood vessels, which is essential in various diseases, including cancer.<sup>17</sup> VEGFR-2 is important to cancer progression and development, acting as the primary regulator of angiogenesis.<sup>18</sup> The activation of VEGFR-2 by vascular endothelial growth factor (VEGF) is essential for the launch of tumor angiogenesis.<sup>19</sup> Downstream signaling cascades and particular endothelial activities, such as enhanced permeability of vascular endothelial cells and augmented endothelial proliferation, ultimately result in angiogenesis.<sup>20</sup> Inhibiting the VEGF/VEGFR-2 signaling network is thus an effective therapeutic strategy for suppressing tumor growth.<sup>21</sup> In addition, inhibiting VEGFR-2 has been demonstrated to increase apoptosis in tumor cells, boosting the anticancer effect.<sup>22,23</sup>

Heterocycles, particularly azoles, play a crucial role in contemporary medicinal chemistry due to their numerous applications in drug design and discovery.<sup>24,25</sup> Their potential use in various medical sectors, particularly as anticancer drugs, are being investigated. Thiazole, a five-membered heterocyclic moiety containing sulfur and nitrogen, garnered considerable attention due to its significant biological properties.<sup>26,27</sup> Thiazole and its derivatives represent one of the most potent groups of chemicals, renowned for their extensive range of activities, with anticancer properties being paramount.<sup>28,29</sup> Furthermore, thiazole-containing compounds have been found in a variety of clinically approved anticancer medications, including dasatinib (a tyrosine kinase inhibitor),<sup>30</sup> dabrafenib (an inhibitor BRAF protein kinase),<sup>31</sup> and patellamide A (cytotoxicity against multidrug-resistant malignancy).<sup>32</sup>

Lv *et al.*<sup>33</sup> presented two series of thiazole-derived compounds and evaluated their inhibitory effects on EGFR and HER-2 kinases. Various synthesized compounds exhibited

significant inhibitory effects against EGFR and HER-2. Compound I (Fig. 1) exhibited the highest EGFR and HER-2 inhibitory activity ( $IC_{50} = 0.09 \mu\text{M}$  for EGFR and  $IC_{50} = 0.42 \mu\text{M}$  for HER-2) in breast cancer (MCF-7) cancer cell lines relative to erlotinib. The EGFR molecular docking model revealed that compound I had excellent binding to the hydroxyl group and established hydrogen bonds with Met 769 and Cys 751.

Sabry *et al.* reported a novel series of thiazole-based derivatives as potent anti-proliferative agents for the development of multi-targeting anticancer therapeutics. Compound II (Fig. 1) exhibited the highest antiproliferative efficacy against EGFR ( $IC_{50} = 0.122 \mu\text{M}$ ) and HER-2 ( $IC_{50} = 0.078 \mu\text{M}$ ) kinases, as well as MCF-7 breast cancer. Additionally, compound II was observed to induce cytotoxicity in MCF-7 breast cancer cells through apoptosis and cell cycle arrest at the G1/S phase. Compound II was determined to comply with Lipinski's rule of five and had a favorable ADMET profile. Finally, the molecular modeling investigations of compound II revealed a strong binding affinity for the Lys745 and Arg841 amino acid residues in the EGFR kinase active site, as well as Met801 in the HER-2 kinase active site.<sup>34</sup>

On the other hand, 1,2,3-triazoles are nitrogenous heterocycles characterized by the presence of three nitrogen atoms inside the ring structure. 1,2,3-Triazoles are stable entities that engage with biological targets through hydrogen bond formation, therefore serving as significant scaffolds in pharmaceutical development.<sup>35–38</sup> 1,2,3-Triazoles have been demonstrated to possess anticancer properties through various mechanisms, including their function as tyrosine kinase inhibitors.<sup>39</sup>

In a recent publication from our lab,<sup>39</sup> we described the design and synthesis of a new series of 1,2,3-triazole-based aryl carboximidamide derivatives as antiproliferative agents with multi-targeting inhibitory action. The results revealed that compound III (Fig. 2) is the most potent EGFR/VEGFR-2 inhibitor, with  $IC_{50}$  values of 83 and 1.80 nM against EGFR and VEGFR-2, respectively. The apoptotic markers experiment indicated that compound III significantly elevated caspase-3 and Bax levels while reducing the anti-apoptotic Bcl-2 protein levels. The ADMET of compound III demonstrated safety and an excellent pharmacokinetic profile.

In another paper,<sup>35</sup> we present the antiproliferative efficacy of new 1,2,3-triazole/quinoline hybrids as multi-target



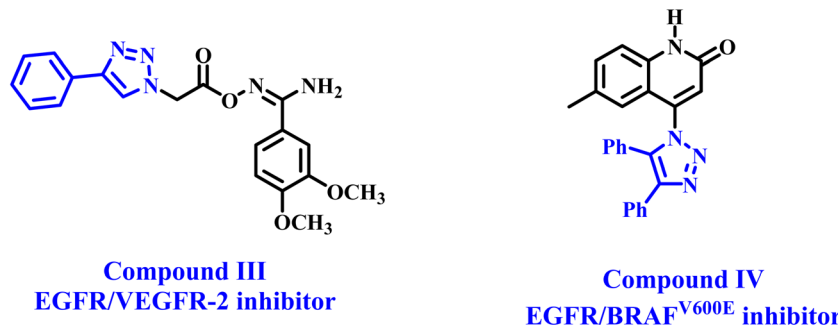


Fig. 2 Structures of 1,2,3-triazole-based anticancer agents III and IV.

inhibitors of EGFR, BRAF<sup>V600E</sup>, and EGFR<sup>T790M</sup>. Compound IV (Fig. 2) exhibited the highest inhibitory potency against the examined molecular targets, with IC<sub>50</sub> values of 57, 68, and 9.70 nM, respectively. The apoptotic assay results indicated that compound IV acts as an activator of caspase-3, caspase-8, and Bax, while also serving as a down-regulator of the antiapoptotic protein Bcl-2. Compound IV exhibited notable antioxidant activity at 10  $\mu$ M, demonstrating DPPH radical scavenging of 73.5%, compared to Trolox's 77.6%.

Inspired by prior data and as part of our ongoing efforts to identify a dual or multi-targeted antiproliferative agent,<sup>35,40–45</sup> we present the design, synthesis, and antiproliferative efficacy of a novel series of thiazole/1,2,3-triazole hybrids (**10a–o**, Fig. 3) as multi-targeted inhibitors. The new compounds **10a–o** are composed of thiazole and 1,2,3-triazole moieties, which, as indicated in the introduction, are known as antiproliferative agents that inhibit RTKs such as EGFR, HER-2, VEGFR-2, and the protein kinase BRAF<sup>V600E</sup>. The novel compounds also integrate the chalcone moiety, which is widely known for its anti-cancer effects, with the intention of increasing antiproliferative activity.<sup>46,47</sup> The selection of various substituents (R<sub>1</sub> and R<sub>2</sub>), whether as electron-withdrawing or electron-donating groups or atoms, to examine the influence of their electronic effects. All the newly synthesized compounds were validated by <sup>1</sup>H NMR, <sup>13</sup>C NMR, and elemental microanalysis.

The newly synthesized compounds were evaluated for their antiproliferative efficiency against a panel of four cancer cell lines. The most effective antiproliferative agents were

subsequently evaluated as inhibitors of EGFR, BRAF<sup>V600E</sup>, HER-2, and VEGFR-2. Moreover, the apoptotic potential of the most potent derivatives against Bcl-2, p53, and Bax were examined. Finally, *in silico* studies were performed to investigate the binding interactions with the targeted receptors, as well as the pharmacokinetic properties of the new compounds.

## 2. Experimental

### 2.1. Chemistry

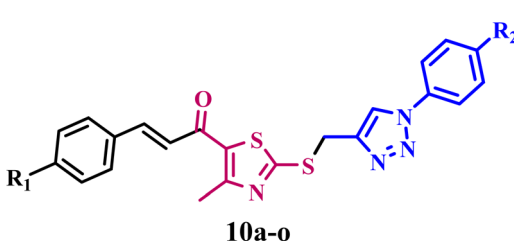
General details: refer to Appendix A (SI File).

**2.1.1. General procedure for the synthesis of compounds (6a–e).** A mixture of thiazole chalcones **5a–e** (4 mmol), propargyl bromide (4 mmol; 476 mg), anhydrous sodium carbonate (6 mmol; 636 mg), and sodium iodide (8 mmol, 1.2 g) in acetone was stirred at room temperature for 6 h. The solvent was evaporated under reduced pressure, and the formed precipitate was thoroughly washed with a 10% sodium thiosulfate solution and distilled water. The product was then recrystallized from ethanol.

**2.1.1.1. (E)-1-(4-Methyl-2-(prop-2-yn-1-ylthio)thiazol-5-yl)-3-phenylprop-2-en-1-one (6a).** Yellow crystals; 0.983 g, 82% yield; mp 177–179 °C; <sup>1</sup>H NMR (400 MHz, DMSO-*d*<sub>6</sub>)  $\delta$  7.81 (dd, *J* = 6.7, 2.9 Hz, 2H), 7.70 (d, *J* = 15.5 Hz, 1H), 7.47–7.46 (m, 3H), 7.39 (d, *J* = 15.5 Hz, 1H), 4.20 (d, *J* = 2.6 Hz, 2H), 3.35 (t, *J* = 2.6 Hz, 1H), 2.70 (s, 3H); <sup>13</sup>C NMR (100 MHz, DMSO-*d*<sub>6</sub>)  $\delta$  181.98, 167.99, 158.55, 144.26, 134.62, 132.81, 131.39, 129.50, 129.32, 124.80, 79.27, 75.46, 22.03, 18.77; anal. calcd. For C<sub>16</sub>H<sub>13</sub>NOS<sub>2</sub>: C, 64.19%; H, 4.38%; N, 4.68%. Found: C, 64.29%; H, 4.32%; N, 4.75%.

**2.1.1.2. (E)-3-(4-Chlorophenyl)-1-(4-methyl-2-(prop-2-yn-1-ylthio)thiazol-5-yl)prop-2-en-1-one (6b).** Yellow crystals; 1.042 g, 78% yield; mp 183–184 °C; <sup>1</sup>H NMR (400 MHz, DMSO-*d*<sub>6</sub>)  $\delta$  7.85 (d, *J* = 8.5 Hz, 2H), 7.68 (d, *J* = 15.6 Hz, 1H), 7.52 (d, *J* = 8.5 Hz, 2H), 7.41 (d, *J* = 15.5 Hz, 1H), 4.20 (d, *J* = 2.6 Hz, 2H), 3.35 (t, *J* = 2.6 Hz, 1H), 2.70 (s, 3H); <sup>13</sup>C NMR (100 MHz, DMSO-*d*<sub>6</sub>)  $\delta$  181.82, 168.12, 158.72, 142.77, 135.87, 133.58, 132.70, 131.02, 129.52, 125.48, 79.25, 75.45, 22.04, 18.77; anal. calcd. For C<sub>16</sub>H<sub>12</sub>ClNOS<sub>2</sub>: C, 57.56%; H, 3.62%; N, 4.20%. Found: C, 57.71%; H, 3.55%; N, 4.18%.

**2.1.1.3. (E)-3-(4-Fluorophenyl)-1-(4-methyl-2-(prop-2-yn-1-ylthio)thiazol-5-yl)prop-2-en-1-one (6c).** Yellow crystals; 1.016 g, 80% yield; mp 180–182 °C; <sup>1</sup>H NMR (400 MHz, DMSO-*d*<sub>6</sub>)  $\delta$  7.90



**R<sub>1</sub> = H, Cl, F, and OMe**  
**R<sub>2</sub> = H, Cl, and OMe**

Fig. 3 Structures of the new compounds **10a–o**.



(dd,  $J = 8.7, 5.6$  Hz, 2H), 7.70 (d,  $J = 15.5$  Hz, 1H), 7.37–7.28 (m, 3H), 4.19 (d,  $J = 2.6$  Hz, 2H), 3.35 (t,  $J = 2.6$  Hz, 1H), 2.69 (s, 3H);  $^{13}\text{C}$  NMR (100 MHz, DMSO- $d_6$ )  $\delta$  181.42, 167.51, 164.80, 162.32, 158.10, 142.59, 132.29, 131.24, 124.18, 116.16, 78.79, 74.97, 21.55, 18.28; anal. calcd. For  $\text{C}_{16}\text{H}_{12}\text{FNOS}_2$ : C, 60.55%; H, 3.81%; N, 4.41%. Found: C, 60.68%; H, 3.70%; N, 4.52%.

**2.1.1.4.** *(E)-1-(4-Methyl-2-(prop-2-yn-1-ylthio)thiazol-5-yl)-3-(p-tolyl)prop-2-en-1-one (6d).* Yellow crystals; 1.066 g, 85% yield; mp 187–188 °C;  $^1\text{H}$  NMR (400 MHz, DMSO- $d_6$ )  $\delta$  7.72–7.66 (m, 3H), 7.34 (d,  $J = 15.5$  Hz, 1H), 7.28 (d,  $J = 7.7$  Hz, 2H), 4.20 (d,  $J = 2.0$  Hz, 2H), 3.36 (s, 1H), 2.70 (s, 3H), 2.36 (s, 3H);  $^{13}\text{C}$  NMR (100 MHz, DMSO- $d_6$ )  $\delta$  181.86, 167.55, 162.15, 158.13, 143.53, 134.62, 131.38, 128.67, 122.17, 115.32, 79.36, 75.34, 21.95, 21.58, 18.78; anal. calcd. For  $\text{C}_{17}\text{H}_{15}\text{NOS}_2$ : C, 65.15%; H, 4.82%; N, 4.47%. Found: C, 65.25%; H, 4.75%; N, 4.52%.

**2.1.1.5.** *(E)-3-(4-Methoxyphenyl)-1-(4-methyl-2-(prop-2-yn-1-ylthio)thiazol-5-yl)prop-2-en-1-one (6e).* Brown crystals; 1.068 g, 81% yield; mp 192–194 °C;  $^1\text{H}$  NMR (400 MHz, DMSO- $d_6$ )  $\delta$  7.77 (d,  $J = 8.6$  Hz, 2H), 7.66 (d,  $J = 15.4$  Hz, 1H), 7.23 (d,  $J = 15.4$  Hz, 1H), 7.01 (d,  $J = 8.6$  Hz, 2H), 4.18 (d,  $J = 2.4$  Hz, 2H), 3.82 (s, 3H), 2.68 (s, 3H);  $^{13}\text{C}$  NMR (100 MHz, DMSO- $d_6$ )  $\delta$  181.83, 167.53, 162.10, 158.19, 144.38, 132.93, 131.30, 127.15, 122.14, 115.00, 79.30, 75.32, 55.87, 21.99, 18.66; anal. calcd. For  $\text{C}_{17}\text{H}_{15}\text{NO}_2\text{S}_2$ : C, 61.98%; H, 4.59%; N, 4.25%. Found: C, 61.87%; H, 4.68%; N, 4.16%.

**2.1.2. General procedure for the synthesis of compounds (9a–c).**<sup>48</sup> Aniline derivatives 7a–c (1 mmol) were dissolved in 15 mL of distilled water containing 10 mL of concentrated HCl and cooled in an ice bath. Then a solution of sodium nitrite (1.3 mmol, 90 mg) in water was added dropwise over 15 min, and the mixture was stirred for an additional 30 min at 0 °C to complete diazotization. Subsequently, a solution of sodium azide (1.3 mmol, 85 mg) in water was added dropwise over 15 min, and the reaction mixture was stirred for 2 h at 0 °C. The formed azides were extracted with methylene chloride (3 × 20 mL), and the combined organic layers were dried over anhydrous sodium sulfate, filtered, and concentrated under reduced pressure to afford the corresponding azides 9a–c as yellow oils which were used directly in the next step without further purification. The procedure was adapted from reported methods.<sup>48</sup>

**2.1.3. General procedure for the synthesis of compounds (10a–o).** Compounds 6a–e (1 mmol) and aromatic azides 9a–c (1.1 mmol) were dissolved in a 1 : 1 THF water mixture (20 mL). Then, sodium (L)-ascorbate (99 mg, 0.5 mmol) and copper sulfate (25 mg, 0.1 mmol) were added portion-wise. The reaction mixture was stirred at room temperature for 5 h. The formed precipitate was filtered off, washed with water, and then recrystallized from absolute ethanol.

**2.1.3.1. *(E)-1-(4-Methyl-2-(((1-phenyl-1H-1,2,3-triazol-4-yl)methyl)thio)thiazol-5-yl)-3-phenylprop-2-en-1-one (10a).*** Yellow powder; 0.298 g, 71% yield; mp 223–224 °C;  $^1\text{H}$  NMR (400 MHz, DMSO- $d_6$ )  $\delta$  8.84 (s, 1H), 7.90 (d,  $J = 8.0$  Hz, 2H), 7.81–7.80 (m, 2H), 7.69 (d,  $J = 15.5$  Hz, 1H), 7.60 (t,  $J = 7.8$  Hz, 2H), 7.51 (d,  $J = 7.4$  Hz, 1H), 7.48–7.46 (m, 3H), 7.38 (d,  $J = 15.5$  Hz, 1H), 4.73 (s, 2H), 2.72 (s, 3H);  $^{13}\text{C}$  NMR (100 MHz, DMSO- $d_6$ )  $\delta$  181.92, 168.56, 158.67, 144.16, 143.69, 136.95, 134.61, 132.37, 131.38, 130.38, 129.49, 129.30, 129.26, 124.89, 122.61, 120.60, 28.33,

18.77; anal. calcd. For  $\text{C}_{22}\text{H}_{18}\text{N}_4\text{OS}_2$ : C, 63.14%; H, 4.34%; N, 13.39%. Found: C, 63.30%; H, 4.43%; N, 13.27%.

**2.1.3.2. *(E)-3-(4-Chlorophenyl)-1-(4-methyl-2-(((1-phenyl-1H-1,2,3-triazol-4-yl)methyl)thio)thiazol-5-yl)prop-2-en-1-one (10b).*** Yellow powder; 0.340 g, 75% yield; mp 221–223 °C;  $^1\text{H}$  NMR (400 MHz, DMSO- $d_6$ )  $\delta$  8.83 (s, 1H), 7.88 (d,  $J = 7.7$  Hz, 2H), 7.84 (d,  $J = 8.5$  Hz, 2H), 7.67 (d,  $J = 15.5$  Hz, 1H), 7.59 (t,  $J = 7.8$  Hz, 2H), 7.52–7.47 (m, 3H), 7.39 (d,  $J = 15.5$  Hz, 1H), 4.72 (s, 2H), 2.71 (s, 3H);  $^{13}\text{C}$  NMR (100 MHz, DMSO- $d_6$ )  $\delta$  181.91, 168.60, 159.70, 158.65, 144.18, 134.60, 133.50, 132.36, 131.38, 130.36, 129.51, 129.32, 125.00, 122.71, 122.34, 115.30, 28.34, 18.74; anal. calcd. For  $\text{C}_{22}\text{H}_{17}\text{ClN}_4\text{OS}_2$ : C, 58.33%; H, 3.78%; N, 12.37%. Found: C, 58.45%; H, 3.68%; N, 12.42%.

**2.1.3.3. *(E)-3-(4-Fluorophenyl)-1-(4-methyl-2-(((1-phenyl-1H-1,2,3-triazol-4-yl)methyl)thio)thiazol-5-yl)prop-2-en-1-one (10c).*** Yellow powder; 0.363 g, 83% yield; mp 236–238 °C;  $^1\text{H}$  NMR (400 MHz, DMSO- $d_6$ )  $\delta$  8.83 (s, 1H), 7.89–7.88 (m, 4H), 7.68 (d,  $J = 15.5$  Hz, 1H), 7.59 (t,  $J = 7.7$  Hz, 2H), 7.48 (t,  $J = 7.3$  Hz, 1H), 7.35–7.27 (m, 3H), 4.72 (s, 2H), 2.71 (s, 3H);  $^{13}\text{C}$  NMR (100 MHz, DMSO- $d_6$ )  $\delta$  181.93, 168.63, 159.78, 158.55, 143.40, 140.35, 134.73, 132.30, 131.72, 131.62, 131.36, 125.04, 123.58, 122.32, 116.33, 114.95, 28.31, 18.74; anal. calcd. For  $\text{C}_{22}\text{H}_{17}\text{FN}_4\text{OS}_2$ : C, 60.53%; H, 3.93%; N, 12.84%. Found: C, 60.61%; H, 4.03%; N, 12.70%.

**2.1.3.4. *(E)-1-(4-Methyl-2-(((1-phenyl-1H-1,2,3-triazol-4-yl)methyl)thio)thiazol-5-yl)-3-(p-tolyl)prop-2-en-1-one (10d).*** Yellow powder; 0.363 g, 74% yield; mp 230–233 °C;  $^1\text{H}$  NMR (400 MHz, DMSO- $d_6$ )  $\delta$  8.84 (s, 1H), 7.90 (d,  $J = 7.9$  Hz, 2H), 7.70–7.64 (m, 3H), 7.60 (t,  $J = 7.7$  Hz, 2H), 7.50 (t,  $J = 7.4$  Hz, 1H), 7.32 (d,  $J = 15.5$  Hz, 1H), 7.27 (d,  $J = 7.9$  Hz, 2H), 4.73 (s, 2H), 2.71 (s, 3H), 2.35 (s, 3H);  $^{13}\text{C}$  NMR (100 MHz, DMSO- $d_6$ )  $\delta$  181.77, 167.99, 162.04, 158.41, 144.35, 143.00, 137.05, 132.62, 132.37, 130.31, 127.01, 124.21, 122.50, 120.96, 114.90, 113.98, 28.28, 21.56, 18.74; anal. calcd. For  $\text{C}_{23}\text{H}_{20}\text{N}_4\text{OS}_2$ : C, 63.86%; H, 4.66%; N, 12.95%. Found: C, 64.02%; H, 4.75%; N, 13.08%.

**2.1.3.5. *(E)-3-(4-Methoxyphenyl)-1-(4-methyl-2-(((1-phenyl-1H-1,2,3-triazol-4-yl)methyl)thio)thiazol-5-yl)prop-2-en-1-one (10e).*** Yellow powder; 0.323 g, 72% yield; mp 242–244 °C;  $^1\text{H}$  NMR (400 MHz, DMSO- $d_6$ )  $\delta$  8.84 (s, 1H), 7.90 (d,  $J = 7.8$  Hz, 2H), 7.77 (d,  $J = 8.6$  Hz, 1H), 7.66 (d,  $J = 15.4$  Hz, 1H), 7.60 (t,  $J = 7.7$  Hz, 2H), 7.50 (t,  $J = 7.3$  Hz, 1H), 7.24 (d,  $J = 15.4$  Hz, 1H), 7.02 (d,  $J = 8.6$  Hz, 2H), 4.73 (s, 2H), 3.83 (s, 3H), 2.71 (s, 3H);  $^{13}\text{C}$  NMR (100 MHz, DMSO- $d_6$ )  $\delta$  181.80, 168.05, 162.09, 158.23, 144.28, 143.74, 136.96, 132.56, 131.30, 130.39, 129.26, 127.22, 122.61, 122.32, 120.60, 115.00, 55.90, 28.33, 18.71; anal. calcd. For  $\text{C}_{23}\text{H}_{20}\text{N}_4\text{O}_2\text{S}_2$ : C, 61.59%; H, 4.49%; N, 12.49%. Found: C, 61.63%; H, 4.57%; N, 12.70%.

**2.1.3.6. *(E)-1-(2-(((1-(4-Chlorophenyl)-1H-1,2,3-triazol-4-yl)methyl)thio)-4-methylthiazol-5-yl)-3-phenylprop-2-en-1-one (10f).*** Yellow powder; 0.318 g, 70% yield; mp 231–232 °C;  $^1\text{H}$  NMR (400 MHz, DMSO- $d_6$ )  $\delta$  8.85 (s, 1H), 7.94 (d,  $J = 8.8$  Hz, 2H), 7.80 (dd,  $J = 6.3, 2.7$  Hz, 2H), 7.70–7.65 (m, 3H), 7.47–7.46 (m, 3H), 7.38 (d,  $J = 15.5$  Hz, 1H), 4.72 (s, 2H), 2.71 (s, 3H);  $^{13}\text{C}$  NMR (100 MHz, DMSO- $d_6$ )  $\delta$  181.96, 168.52, 158.67, 144.19, 143.94, 135.75, 134.61, 133.53, 132.40, 131.40, 130.35, 129.51, 129.31, 124.90, 122.72, 122.32, 28.26, 18.77; anal. calcd. For  $\text{C}_{22}\text{H}_{17}\text{ClN}_4\text{OS}_2$ : C, 61.59%; H, 4.49%; N, 12.49%.



58.33%; H, 3.78%; N, 12.37%. Found: C, 58.17%; H, 3.66%; N, 12.49%.

**2.1.3.7. (E)-3-(4-Chlorophenyl)-1-(2-(((1-(4-chlorophenyl)-1H-1,2,3-triazol-4-yl)methyl)thio)-4-methylthiazol-5-yl)prop-2-en-1-one (10g).** Yellow powder; 0.322 g, 66% yield; mp 233–236 °C; <sup>1</sup>H NMR (400 MHz, DMSO-*d*<sub>6</sub>) δ 8.86 (s, 1H), 7.94 (d, *J* = 6.8 Hz, 2H), 7.85 (d, *J* = 5.9 Hz, 2H), 7.68–7.66 (m, 3H), 7.53 (d, *J* = 3.8 Hz, 2H), 7.40 (d, *J* = 14.3 Hz, 1H), 4.73 (s, 2H), 2.72 (s, 3H); <sup>13</sup>C NMR (100 MHz, DMSO-*d*<sub>6</sub>) δ 181.89, 168.44, 159.79, 144.15, 143.29, 135.40, 133.01, 132.45, 131.39, 130.38, 126.31, 122.29, 121.23, 117.26, 116.05, 114.24, 28.33, 18.72; anal. calcd. For C<sub>22</sub>H<sub>16</sub>Cl<sub>2</sub>N<sub>4</sub>OS<sub>2</sub>: C, 54.21%; H, 3.31%; N, 11.49%. Found: C, 54.35%; H, 3.24%; N, 11.36%.

**2.1.3.8. (E)-1-(2-(((1-(4-Chlorophenyl)-1H-1,2,3-triazol-4-yl)methyl)thio)-4-methylthiazol-5-yl)-3-(4-fluorophenyl)prop-2-en-1-one (10h).** Yellow powder; 0.368 g, 78% yield; mp 243–245 °C; <sup>1</sup>H NMR (400 MHz, DMSO-*d*<sub>6</sub>) δ 8.86 (s, 1H), 7.95–7.90 (m, 4H), 7.70–7.68 (m, 3H), 7.37–7.31 (m, 3H), 4.73 (s, 2H), 2.72 (s, 3H); <sup>13</sup>C NMR (100 MHz, DMSO-*d*<sub>6</sub>) δ 181.89, 168.60, 160.33, 158.42, 143.04, 133.09, 132.33, 131.68, 131.30, 130.42, 126.22, 122.58, 121.29, 116.73, 116.17, 114.89, 28.37, 18.78; anal. calcd. For C<sub>22</sub>H<sub>16</sub>ClFN<sub>4</sub>OS<sub>2</sub>: C, 56.11%; H, 3.42%; N, 11.90%. Found: C, 56.22%; H, 3.50%; N, 11.99%.

**2.1.3.9. (E)-1-(2-(((1-(4-Chlorophenyl)-1H-1,2,3-triazol-4-yl)methyl)thio)-4-methylthiazol-5-yl)-3-(*p*-tolyl)prop-2-en-1-one (10i).** Yellow powder; 0.323 g, 69% yield; mp 234–237 °C; <sup>1</sup>H NMR (400 MHz, DMSO-*d*<sub>6</sub>) δ 8.87 (s, 1H), 7.96–7.93 (m, 2H), 7.69–7.68 (m, 5H), 7.33–7.28 (m, 3H), 4.73 (s, 2H), 2.71 (s, 3H), 2.36 (s, 3H); <sup>13</sup>C NMR (100 MHz, DMSO-*d*<sub>6</sub>) δ 181.80, 168.47, 160.86, 158.31, 144.22, 143.61, 136.93, 134.59, 131.58, 131.20, 130.81, 129.41, 124.62, 122.38, 116.47, 114.26, 28.36, 21.55, 18.78; anal. calcd. For C<sub>23</sub>H<sub>19</sub>ClN<sub>4</sub>OS<sub>2</sub>: C, 59.15%; H, 4.10%; N, 12.00%. Found: C, 59.07%; H, 4.16%; N, 12.10%.

**2.1.3.10. (E)-1-(2-(((1-(4-Chlorophenyl)-1H-1,2,3-triazol-4-yl)methyl)thio)-4-methylthiazol-5-yl)-3-(4-methoxyphenyl)prop-2-en-1-one (10j).** Yellow powder; 0.353 g, 73% yield; mp 222–224 °C; <sup>1</sup>H NMR (400 MHz, DMSO-*d*<sub>6</sub>) δ 8.86 (s, 1H), 7.95–7.94 (m, 2H), 7.77–7.76 (m, 2H), 7.67–7.66 (m, 3H), 7.23 (d, *J* = 14.7 Hz, 2H), 7.02–7.01 (m, 2H), 4.72 (s, 2H), 3.82 (s, 3H), 2.71 (s, 3H); <sup>13</sup>C NMR (100 MHz, DMSO-*d*<sub>6</sub>) δ 181.78, 167.98, 162.09, 158.22, 144.27, 143.96, 135.75, 133.51, 132.57, 131.29, 130.33, 127.21, 122.69, 122.29, 114.99, 114.23, 55.89, 28.26, 18.71; anal. calcd. For C<sub>23</sub>H<sub>19</sub>ClN<sub>4</sub>O<sub>2</sub>S<sub>2</sub>: C, 57.20%; H, 3.97%; N, 11.60%. Found: C, 57.27%; H, 4.11%; N, 11.69%.

**2.1.3.11. (E)-1-(2-(((1-(4-Methoxyphenyl)-1H-1,2,3-triazol-4-yl)methyl)thio)-4-methylthiazol-5-yl)-3-phenylprop-2-en-1-one (10k).** Yellow powder; 0.301 g, 67% yield; mp 220–221 °C; <sup>1</sup>H NMR (400 MHz, DMSO-*d*<sub>6</sub>) δ 8.73 (s, 1H), 7.81–7.79 (m, 4H), 7.69 (d, *J* = 15.5 Hz, 1H), 7.48 (s, 3H), 7.39 (d, *J* = 15.6 Hz, 1H), 7.13 (d, *J* = 8.3 Hz, 2H), 4.71 (s, 2H), 3.83 (s, 3H), 2.72 (s, 3H); <sup>13</sup>C NMR (100 MHz, DMSO-*d*<sub>6</sub>) δ 181.93, 168.62, 159.80, 158.67, 144.17, 134.62, 132.36, 131.47, 131.38, 130.38, 129.50, 129.31, 124.91, 122.59, 122.28, 115.35, 56.04, 28.38, 18.77; anal. calcd. For C<sub>23</sub>H<sub>20</sub>N<sub>4</sub>O<sub>2</sub>S<sub>2</sub>: C, 61.59%; H, 4.49%; N, 12.49%. Found: C, 61.43%; H, 4.58%; N, 12.35%.

**2.1.3.12. (E)-3-(4-Chlorophenyl)-1-(2-(((1-(4-methoxyphenyl)-1H-1,2,3-triazol-4-yl)methyl)thio)-4-methylthiazol-5-yl)prop-2-en-**

**1-one (10l).** Yellow powder; 0.411 g, 85% yield; mp 241–243 °C; <sup>1</sup>H NMR (400 MHz, DMSO-*d*<sub>6</sub>) δ 8.71 (s, 1H), 7.84 (d, *J* = 8.4 Hz, 2H), 7.78 (d, *J* = 9.0 Hz, 2H), 7.66 (d, *J* = 15.5 Hz, 1H), 7.52 (d, *J* = 8.4 Hz, 2H), 7.39 (d, *J* = 15.5 Hz, 1H), 7.12 (d, *J* = 9.0 Hz, 2H), 4.70 (s, 2H), 3.82 (s, 3H), 2.70 (s, 3H); <sup>13</sup>C NMR (100 MHz, DMSO-*d*<sub>6</sub>) δ 181.84, 168.10, 159.79, 158.24, 143.92, 139.81, 136.96, 135.48, 131.45, 130.38, 127.23, 125.05, 122.71, 122.43, 116.77, 114.35, 56.05, 28.37, 18.75; anal. calcd. For C<sub>23</sub>H<sub>19</sub>ClN<sub>4</sub>O<sub>2</sub>S<sub>2</sub>: C, 57.20%; H, 3.97%; N, 11.60%. Found: C, 57.12%; H, 4.07%; N, 11.47%.

**2.1.3.13. (E)-3-(4-Fluorophenyl)-1-(2-(((1-(4-methoxyphenyl)-1H-1,2,3-triazol-4-yl)methyl)thio)-4-methylthiazol-5-yl)prop-2-en-1-one (10m).** Yellow powder; 0.378 g, 81% yield; mp 228–230 °C; <sup>1</sup>H NMR (400 MHz, DMSO-*d*<sub>6</sub>) δ 8.72 (s, 1H), 7.89 (dd, *J* = 8.2, 5.8 Hz, 2H), 7.79 (d, *J* = 8.9 Hz, 2H), 7.69 (d, *J* = 15.5 Hz, 1H), 7.36–7.28 (m, 3H), 7.12 (d, *J* = 8.9 Hz, 2H), 4.70 (s, 2H), 3.82 (s, 3H), 2.71 (s, 3H); <sup>13</sup>C NMR (100 MHz, DMSO-*d*<sub>6</sub>) δ 181.87, 168.64, 159.80, 158.69, 142.97, 132.32, 131.78, 131.69, 131.32, 130.36, 124.79, 122.58, 122.28, 116.64, 116.42, 115.36, 56.04, 28.37, 18.76; anal. calcd. For C<sub>23</sub>H<sub>19</sub>FN<sub>4</sub>O<sub>2</sub>S<sub>2</sub>: C, 59.21%; H, 4.11%; N, 12.01%. Found: C, 59.39%; H, 4.02%; N, 12.18%.

**2.1.3.14. (E)-1-(2-(((1-(4-Methoxyphenyl)-1H-1,2,3-triazol-4-yl)methyl)thio)-4-methylthiazol-5-yl)-3-(*p*-tolyl)prop-2-en-1-one (10n).** Yellow powder; 0.357 g, 77% yield; mp 235–236 °C; <sup>1</sup>H NMR (400 MHz, DMSO-*d*<sub>6</sub>) δ 8.73 (s, 1H), 7.90 (d, *J* = 8.4 Hz, 2H), 7.78 (d, *J* = 9.0 Hz, 2H), 7.65 (d, *J* = 15.5 Hz, 1H), 7.34 (d, *J* = 15.5 Hz, 1H), 7.27 (d, *J* = 9.0 Hz, 2H), 7.12 (d, *J* = 8.4 Hz, 2H), 4.72 (s, 2H), 3.82 (s, 3H), 2.71 (s, 3H), 2.36 (s, 3H); <sup>13</sup>C NMR (100 MHz, DMSO-*d*<sub>6</sub>) δ 181.78, 168.55, 161.12, 158.70, 144.34, 143.73, 137.80, 134.61, 131.47, 131.22, 130.31, 129.50, 123.59, 120.17, 116.39, 113.81, 56.05, 28.32, 21.54, 18.77; anal. calcd. For C<sub>24</sub>H<sub>22</sub>N<sub>4</sub>O<sub>2</sub>S<sub>2</sub>: C, 62.32%; H, 4.79%; N, 12.11%. Found: C, 62.25%; H, 4.93%; N, 12.20%.

**2.1.3.15. (E)-3-(4-Methoxyphenyl)-1-(2-(((1-(4-methoxyphenyl)-1H-1,2,3-triazol-4-yl)methyl)thio)-4-methylthiazol-5-yl)prop-2-en-1-one (10o).** Yellow powder; 0.393 g, 82% yield; mp 227–228 °C; <sup>1</sup>H NMR (400 MHz, DMSO-*d*<sub>6</sub>) δ 8.72 (s, 1H), 7.78 (t, *J* = 9.0 Hz, 4H), 7.66 (d, *J* = 15.4 Hz, 1H), 7.23 (d, *J* = 15.4 Hz, 1H), 7.12 (d, *J* = 8.8 Hz, 2H), 7.01 (d, *J* = 8.4 Hz, 2H), 4.70 (s, 2H), 3.82 (s, 6H), 2.70 (s, 3H); <sup>13</sup>C NMR (100 MHz, DMSO-*d*<sub>6</sub>) δ 181.89, 168.29, 161.17, 158.60, 144.19, 143.06, 137.01, 132.54, 131.30, 130.32, 129.56, 124.67, 122.29, 120.34, 116.24, 113.19, 56.04, 55.93, 28.32, 18.79; anal. calcd. For C<sub>24</sub>H<sub>22</sub>N<sub>4</sub>O<sub>3</sub>S<sub>2</sub>: C, 60.23%; H, 4.63%; N, 11.71%. Found: C, 60.15%; H, 4.75%; N, 11.60%.

## 2.2. Biology

**2.2.1. Cell viability assay.** The human mammary (MCF-10A) gland epithelial normal cell line was used to assess the effects of compounds **10a–o** on cell viability. Following a 4-day incubation period on MCF-10A cells, the cell viability of **10a–o** was assessed using the MTT test.<sup>49,50</sup> For further information, see Appendix A.

**2.2.2. Antiproliferative assay.** The antiproliferative effect of **10a–o** was assessed using the MTT assay on four human cancer cell lines: MCF-7 for breast cancer, A-549 for lung cancer, Panc-1 for pancreatic cancer, and HT-29 for colon cancer. All cell lines were obtained from ATCC (American Type Cell Culture).



Erlotinib served as a ref. 51 and 52. Using dose-response tests, the  $IC_{50}$  values for novel compounds were determined. Three replicates of each concentration were used in at least two independent experiments, yielding the reported values. Appendix A (SI File) contains experimental details.

**2.2.3. EGFR inhibitory assay.** The EGFR-TK assay was employed to evaluate the inhibitory effectiveness of the most potent derivatives, **10c**, **10e**, **10k**, **10m**, **10n** and **10o**, against EGFR, using erlotinib as the reference compound.<sup>53,54</sup> Appendix A (SI File) contains experimental details.

**2.2.4. HER-2 inhibitory assay.** Using the kinase assay,<sup>45</sup> the compounds **10c**, **10e**, **10k**, **10m**, **10n**, and **10o** were evaluated for their capacity to inhibit HER-2. Lapatinib was the reference substance. Refer to Appendix A for further information.

**2.2.5. BRAF<sup>V600E</sup> inhibitory assay.** An *in vitro* investigation evaluated the efficacy of derivatives **10c**, **10e**, and **10k** as inhibitors of BRAF<sup>V600E</sup>. Vemurafenib served as the reference medication.<sup>55</sup> Refer to Appendix A for additional experimental details.

**2.2.6. VEGFR-2 inhibitory assay.** The inhibitory effects of compounds **10c**, **10e**, and **10k** on VEGFR-2 were evaluated by kinase assays, with Sorafenib as the control drug.<sup>21</sup> Refer to Appendix A for additional experimental details.

**2.2.7. Apoptotic markers assays.** Compounds **10e** and **10k** were assessed for their capacity to induce apoptosis in MCF-7 breast cancer cells by examining the expression of crucial

apoptotic markers, namely Bcl-2, p53, and Bax.<sup>56</sup> For details of all experimental studies, see Appendix A (SI File).

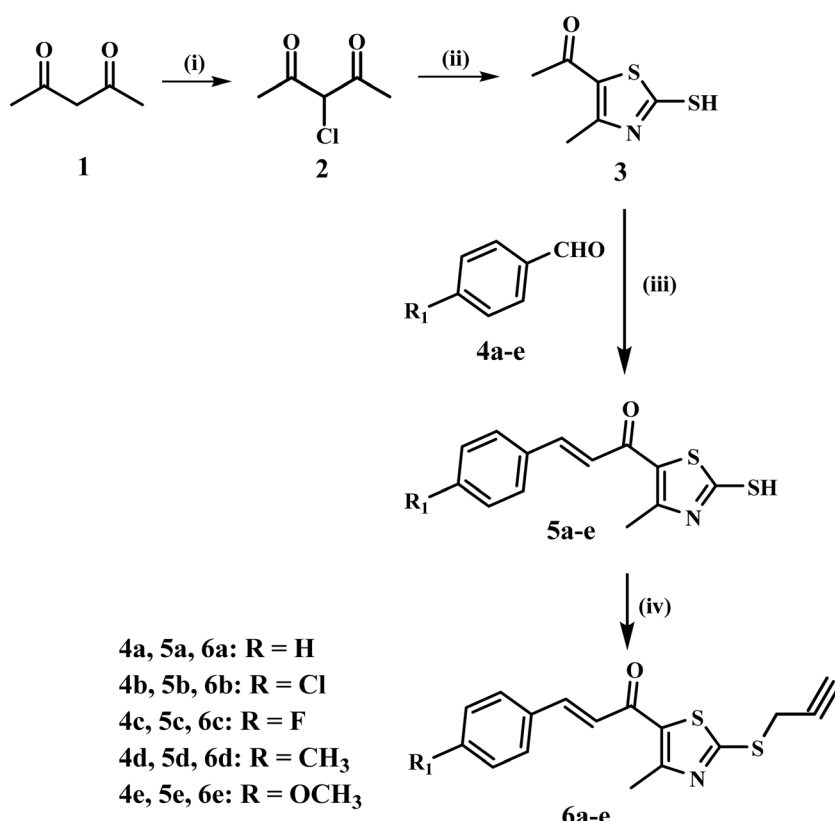
### 2.3. *In silico* studies

For details of all *in silico* studies, see Appendix A (SI File).

## 3. Results and discussion

### 3.1. Chemistry

Scheme 1 depicts the steps in the synthesis of intermediates **6a–e**. The procedure begins with the reaction of acetylacetone (**1**) with sulfonyl chloride in toluene at 0 °C for 12 hours, resulting in the selective chlorination of the active methylene group of acetylacetone to yield compound **2**.<sup>57</sup> The chlorinated product **2** reacts with ammonia and carbon disulfide in ethanol at room temperature for six hours, making the thiazole intermediate **3**. This reaction has a moderate yield of 69%. Subsequently, thiazole **3** undergoes a reaction with the corresponding aldehydes **4a–e** in basic conditions within ethanol at 0 °C for 18 hours. The Claisen–Schmidt condensation effectively generates thiazole chalcones **5a–e** with yields varying from good to excellent (63% to 91%).<sup>58</sup> The thiazole chalcones (**5a–e**) undergo *S*-alkylation with propargyl bromide in the presence of sodium carbonate and sodium iodide in acetone at ambient temperature for six hours. This phase provides the new intermediates **6a–e** in good yields (78–85%).<sup>59</sup>



**Scheme 1** Synthesis of key intermediates **6a–e**. Reagents and conditions: (i)  $SO_2Cl_2$ , toluene, 0 °C, 12 h; (ii)  $NH_3$ ,  $CS_2$ , EtOH, rt, 6 h; (iii) appropriate aromatic aldehyde, 60% NaOH, EtOH, 0 °C, 18 h; (iv) propargyl bromide,  $Na_2CO_3$ ,  $NaI$ , acetone, rt, 6 h.

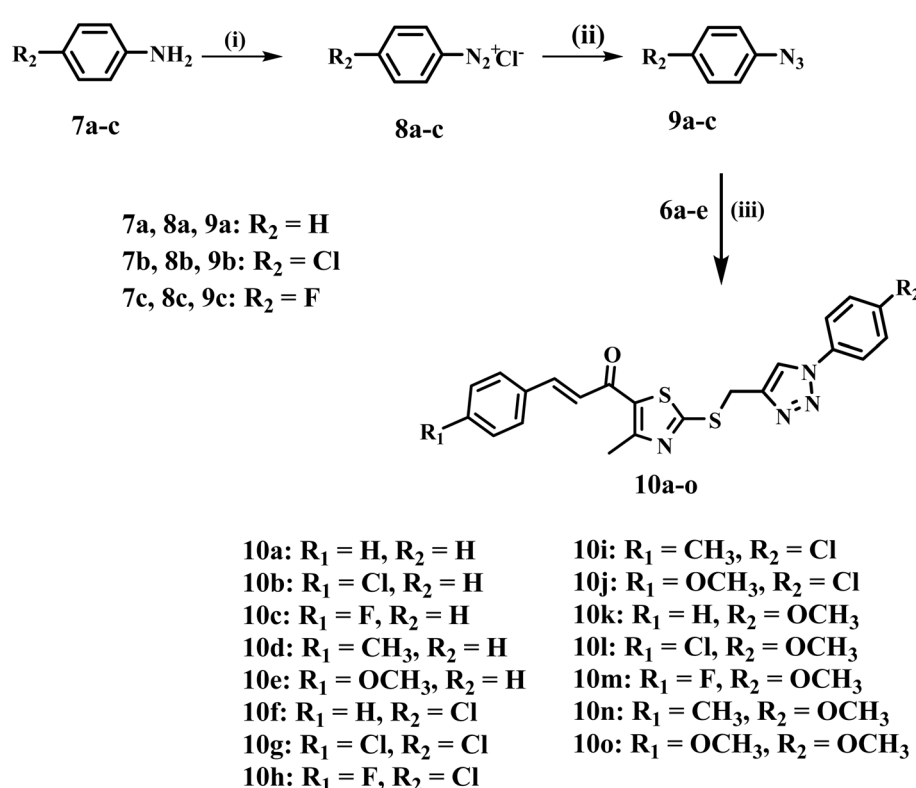


Compounds **6a–e** were characterized *via*  $^1\text{H}$  NMR,  $^{13}\text{C}$  NMR, and elemental analysis. The  $^1\text{H}$  NMR spectra of compounds **6a–e** showed different signals, revealing their structural properties. The absence of the NH proton at  $\delta \sim 13.6$  ppm in compounds **5a–e**, together with the presence of an alkyne proton, is corroborated by a distinctive triplet signal at  $\delta 3.34\text{--}3.36$  ppm ( $J = 2.6$  Hz), indicating the terminal acetylene group inserted during the *S*-alkylation process. The doublet signal at  $\delta 4.18\text{--}4.20$  ppm corresponds to the methylene group adjacent to the sulfur bridge. The  $^{13}\text{C}$  NMR spectra also showed characteristic signals including two distinct signals at  $\delta 78.78\text{--}79.36$  ppm and  $74.97\text{--}75.46$  ppm represent the two sp carbons of the alkyne group introduced during the *S*-alkylation step. The methylene group adjacent to the sulfur bridge appears at  $\delta 21.55\text{--}22.04$  ppm.

Scheme 2 describes the synthesis of the desired compounds **10a–o**. The synthesis involves the diazotization of aniline derivatives **7a–c** into their corresponding diazonium salts **8a–c** using sodium nitrite and hydrochloric acid at  $0\text{ }^\circ\text{C}$ . The procedure occurs effectively under mild conditions. The diazonium salts are subsequently reacted with sodium azide in an acidic environment at the same temperature, yielding azide derivatives **9a–c**.<sup>48</sup> In the final phase, azides **9a–c** are subjected to a reaction with propargyl-functionalized thiazole intermediates **6a–e** under copper(i)-catalyzed azide–alkyne cycloaddition (CuAAC) conditions. The click reaction, catalyzed by  $\text{CuSO}_4$  and sodium ascorbate in THF at ambient temperature, proceeds efficiently, yielding the regioselective synthesis of the desired 1,2,3-triazole derivatives **10a–o** with good yields (66–85%).

The structures of **10a–o** were confirmed using  $^1\text{H}$  NMR,  $^{13}\text{C}$  NMR, and elemental analysis. The  $^1\text{H}$  NMR spectra of the 1,2,3-triazoles **10a–o** exhibited a new singlet signal at  $\delta \sim 8.71\text{--}8.87$  ppm for the triazole CH proton, accompanied by the absence of the terminal alkyne proton ( $\delta \sim 3.34\text{--}3.36$  ppm), and a down-field shift of the methylene protons adjacent to sulfur to  $\delta \sim 4.70\text{--}4.73$  ppm, indicative of the deshielding effect of the triazole ring. Furthermore, in the  $^{13}\text{C}$  NMR, the absence of alkyne carbon signals confirmed cycloaddition, while the methylene carbon was observed at  $\delta \sim 28$  ppm. The distinctive proton signals for the thiazole methyl group and chalcone protons were mostly unchanged, so demonstrating the integrity of these moieties.

The  $^1\text{H}$  NMR spectrum of compound **10l**, for example, exhibits characteristic signals, including a singlet at 2.70 ppm for the methyl group on the thiazole ring and another singlet at 3.82 ppm for the methoxy group. The methylene group is seen as a singlet at 4.70 ppm. The chalcone protons are apparent as two separate doublets at 7.39 ppm and 7.69 ppm. In contrast, the successful cyclization of the triazole ring is indicated by the CH proton, which appears as a singlet at 8.71 ppm. The  $^{13}\text{C}$  NMR spectrum of compound **10l** showed a signal at  $\delta 181.84$  ppm corresponding to the carbonyl group, while the methoxy group gave a signal at  $\delta 56.05$  ppm. The methylene group appeared at  $\delta 28.37$  ppm, and the methyl group on the thiazole ring was observed at  $\delta 18.75$  ppm. Importantly, the disappearance of the alkyne signals at  $\delta 79.30$  ppm and 75.32 ppm, which were present in the starting material **6b** used for the synthesis of **10l**, confirms the successful cyclization.



**Scheme 2** Synthesis of target compounds **10a–o**. Reagents and conditions: (i)  $\text{NaNO}_2$ ,  $\text{HCl}$ ,  $0\text{ }^\circ\text{C}$ , 30 min; (ii)  $\text{NaN}_3$ ,  $\text{HCl}$ ,  $0\text{ }^\circ\text{C}$ , 2 h; (iii)  $\text{CuSO}_4\cdot5\text{H}_2\text{O}$ , Na ascorbate, THF, rt, 5 h.



### 3.2. Biology

**3.2.1. Cell viability assay.** This study investigates the effects of the novel compounds **10a–o** on normal cell lines to assess their safety. The normal human mammary gland epithelial MCF-10A cell line was used to assess the viability of the examined compounds. Cell viability was assessed using the MTT test after four days of incubation of MCF-10A cells with 50  $\mu$ M of each examined compound.<sup>49,50</sup> Table 1 results indicate that none of the tested compounds exhibited cytotoxicity, with all compounds maintaining cell viability above 87% at a concentration of 50  $\mu$ M.

**3.2.2. Antiproliferative assay.** The MTT assay<sup>51,52</sup> was employed to assess the antiproliferative efficacy of novel compounds **10a–o** against four human cancer cell lines, including erlotinib as a control: colon (HT-29), pancreatic (Panc-1), lung (A-549), and breast (MCF-7) cancer cell lines. Table 1 displays the median inhibitory concentration ( $IC_{50}$ ) for

**Table 1**  $IC_{50}$  values of compounds **10a–o** and erlotinib against four cancer cell lines

Comp.	Cell viability %	Antiproliferative activity $IC_{50} \pm SEM$ (nM)				Average ( $IC_{50}$ )
		A-549	MCF-7	Panc-1	HT-29	
<b>10a</b>	90	45 $\pm$ 4	41 $\pm$ 3	48 $\pm$ 4	48 $\pm$ 4	46
<b>10b</b>	89	55 $\pm$ 5	51 $\pm$ 5	58 $\pm$ 5	58 $\pm$ 5	56
<b>10c</b>	88	30 $\pm$ 2	26 $\pm$ 2	30 $\pm$ 2	32 $\pm$ 2	30
<b>10d</b>	91	43 $\pm$ 3	38 $\pm$ 3	44 $\pm$ 4	42 $\pm$ 3	42
<b>10e</b>	90	27 $\pm$ 2	24 $\pm$ 2	28 $\pm$ 2	28 $\pm$ 2	27
<b>10f</b>	92	56 $\pm$ 5	54 $\pm$ 5	58 $\pm$ 5	58 $\pm$ 5	57
<b>10g</b>	89	62 $\pm$ 6	60 $\pm$ 6	64 $\pm$ 6	64 $\pm$ 6	63
<b>10h</b>	93	66 $\pm$ 6	62 $\pm$ 6	69 $\pm$ 6	68 $\pm$ 6	66
<b>10i</b>	91	36 $\pm$ 3	32 $\pm$ 3	38 $\pm$ 3	38 $\pm$ 3	36
<b>10j</b>	90	50 $\pm$ 4	46 $\pm$ 4	52 $\pm$ 4	52 $\pm$ 4	50
<b>10k</b>	87	24 $\pm$ 2	21 $\pm$ 2	26 $\pm$ 2	26 $\pm$ 2	24
<b>10l</b>	92	51 $\pm$ 4	47 $\pm$ 4	53 $\pm$ 5	54 $\pm$ 5	51
<b>10m</b>	87	40 $\pm$ 3	35 $\pm$ 3	40 $\pm$ 3	41 $\pm$ 3	39
<b>10n</b>	90	33 $\pm$ 3	30 $\pm$ 2	36 $\pm$ 3	36 $\pm$ 3	34
<b>10o</b>	91	31 $\pm$ 2	28 $\pm$ 2	32 $\pm$ 2	34 $\pm$ 3	31
Erlotinib	ND	30 $\pm$ 3	40 $\pm$ 3	30 $\pm$ 3	30 $\pm$ 3	33

each compound across all examined cancer cell lines, as well as the  $GI_{50}$  (mean  $IC_{50}$ ), which represents the average of the  $IC_{50}$  values for the four cancer cell lines.

The examined compounds **10a–o** exhibited remarkable antiproliferative activity, with  $GI_{50}$  values ranging from 24 nM to 66 nM against the four assessed cancer cell lines, in contrast to the standard Erlotinib, which demonstrated a  $GI_{50}$  value of 33 nM. Remarkably, all evaluated compounds exhibited a greater affinity for the breast cancer (MCF-7) cell line compared to the other cell lines studied. Compounds **10c**, **10e**, **10k**, **10m**, **10n**, and **10o** were identified as the six most potent derivatives, with  $GI_{50}$  values ranging from 24 nM to 39 nM. In particular, compounds **10c**, **10e**, **10k**, and **10o** ( $GI_{50}$  values of 30, 27, 24, and 31, respectively) demonstrated greater potency than Erlotinib ( $GI_{50}$  value of 33 nM).

All six compounds exhibited greater potency than erlotinib against the MCF-7 breast cancer cell lines, with  $IC_{50}$  values ranging from 21 nM to 35 nM, compared to erlotinib's  $IC_{50}$  value of 40 nM, demonstrating at least a 1.2-fold increase in potency over erlotinib (Fig. 4).

Compound **10k** ( $R_1 = H$ ,  $R_2 = OCH_3$ ) exhibited the highest potency among the newly synthesized derivatives **10a–o**, with a  $GI_{50}$  value of 24 nM, which is 1.4-fold superior to the reference erlotinib ( $GI_{50} = 33$  nM) against the four tested cancer cell lines. Moreover, **10k** had an  $IC_{50}$  value of 21 nM against the breast cancer (MCF-7) cell line, which was twice as potent as erlotinib's  $IC_{50}$  value of 40 nM.

Based on the findings, the type of substitution found on both phenyl rings at the chalcone ( $R_1$ ) and 1,2,3-triazole ( $R_2$ ) moieties appears to be critical for activity. For example, compounds **10l** ( $R_1 = Cl$ ,  $R_2 = OCH_3$ ), **10m** ( $R_1 = F$ ,  $R_2 = OCH_3$ ), **10n** ( $R_1 = CH_3$ ,  $R_2 = OCH_3$ ), and **10o** ( $R_1 = OCH_3$ ,  $R_2 = OCH_3$ ), all possessing the same backbone as compound **10k** but differing in substituents ( $R_1$ ) at position 4 of the phenyl group within the chalcone moiety, exhibited  $GI_{50}$  values of 51, 39, 34, and 31, which are 2.2-, 1.6-, 1.4-, and 1.3-fold less potent than **10k**, respectively. These data indicate that substituting the four-position of the phenyl group within the chalcone moiety reduces activity, and that substitutions with electron-donating groups ( $OCH_3$  and  $CH_3$ )

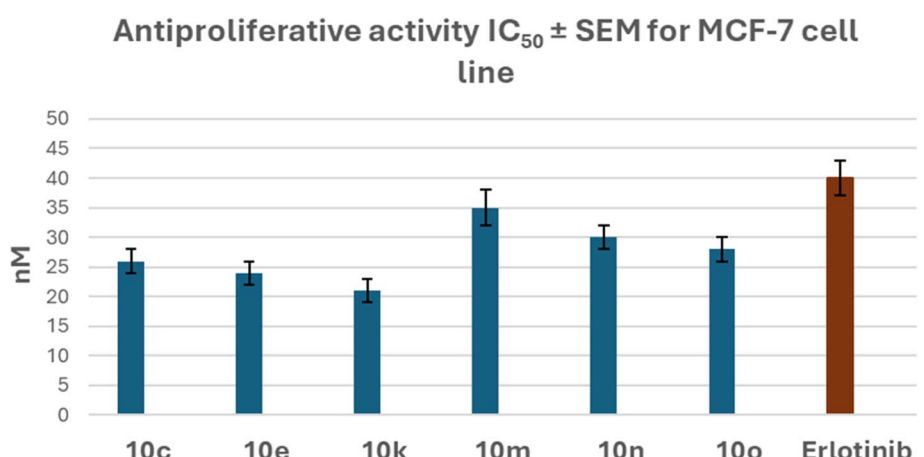


**Fig. 4** Antiproliferative activity ( $IC_{50} \pm SEM$ ) of compounds **10c**, **10e**, **10k**, **10m**, **10n**, and **10o** compared to Erlotinib against the MCF-7 cell line.



are more favorable for antiproliferative activity compared to electron-withdrawing groups (F and Cl).

Compound **10e** ( $R_1 = \text{OCH}_3$ ,  $R_2 = \text{H}$ ) exhibited the second-highest activity, with a  $\text{GI}_{50}$  of 27 nM, slightly less active than **10k** ( $\text{GI}_{50} = 24$  nM), but 1.2-fold more effective than the reference erlotinib ( $\text{GI}_{50} = 33$  nM) against the four tested cancer cell lines. Compound **10e** showed substantial antiproliferative activity against the MCF-7 breast cancer cell line, with an  $\text{IC}_{50}$  value of 24 nM, which is 1.7 times more potent than erlotinib ( $\text{IC}_{50} = 40$  nM).

Also, the four-position substitution of the phenyl group in the 1,2,3-triazole moiety is essential for antiproliferative activity. Compounds **10j** ( $R_1 = \text{OCH}_3$ ,  $R_2 = \text{Cl}$ ) and **10o** ( $R_1 = \text{OCH}_3$ ,  $R_2 = \text{OCH}_3$ ) share the same structure as **10e** ( $R_1 = \text{OCH}_3$ ,  $R_2 = \text{H}$ ) but possess different substituents at the *para* position of the phenyl group of the 1,2,3-triazole moiety ( $R_2$ ), exhibiting  $\text{GI}_{50}$  values of 50 and 31 nM, respectively, which are 1.9- and 1.2-fold less potent than **10e**. The observations suggest that substituting the phenyl group at the four-position of the 1,2,3-triazole moiety lowered activity, with the following order of increasing activity:  $\text{H} > \text{OCH}_3 > \text{Cl}$ . Moreover, these observations provide further evidence that replacement with electron-donating groups is more advantageous for the antiproliferative activity of this class of organic compounds than substitution with electron-withdrawing groups.

Another aspect to consider is the difference in potency between compounds **10a** ( $R_1 = \text{H}$ ,  $R_2 = \text{H}$ ), **10e** ( $R_1 = \text{OCH}_3$ ,  $R_2 = \text{H}$ ), and **10k** ( $R_1 = \text{H}$ ,  $R_2 = \text{OCH}_3$ ). Compound **10a** has a  $\text{GI}_{50}$  value of 46 nM, indicating a potency 1.9-fold and 1.7-fold lower than that of **10k** and **10e**. According to the results, at least one phenyl group must be replaced with a methoxy group, and the optimal combination for activity is an unsubstituted phenyl ring within the chalcone moiety and a *p*-methoxyphenyl group on the 1,2,3-triazole moiety.

Ultimately, compounds **10g** ( $R_1 = \text{Cl}$ ,  $R_2 = \text{Cl}$ ) and **10h** ( $R_1 = \text{F}$ ,  $R_2 = \text{Cl}$ ) had the lowest efficacy, evidenced by their  $\text{GI}_{50}$  values of 63 and 66 nM, respectively. This indicates that electron-withdrawing halogen atoms are not preferred for antiproliferative action.

**3.2.3. EGFR inhibitory assay.** The EGFR-TK assay was employed to evaluate the inhibitory effectiveness of the most

potent derivatives, **10c**, **10e**, **10k**, **10m**, **10n**, and **10o** against EGFR, using erlotinib as the reference compound.<sup>53,54</sup> The  $\text{IC}_{50}$  values (nM) are displayed in Table 2. Compared to the reference erlotinib, which has an  $\text{IC}_{50}$  of 80 nM, the compounds investigated had  $\text{GI}_{50}$  values ranging from 69 to 87 nM, indicating a high level of EGFR inhibitory action.

This *in vitro* experiment matches the antiproliferative assay. The most efficient antiproliferative derivatives, **10e** and **10k**, were also shown to be the best EGFR inhibitors, with  $\text{IC}_{50}$  values of  $73 \pm 4$  and  $69 \pm 4$  nM, respectively, which is 1.2-fold stronger than erlotinib as an EGFR inhibitor. Compounds **10c** and **10o** exhibited strong EGFR inhibitory activity, with  $\text{IC}_{50}$  values of 77 and 79 nM, respectively, which are comparable to that of erlotinib ( $\text{IC}_{50} = 80$  nM). Ultimately, compounds **10m** and **10n** exhibited slightly reduced efficacy relative to erlotinib, with  $\text{IC}_{50}$  values of 83 and 87 nM, respectively. These findings suggest that the studied compounds **10c**, **10e**, **10k**, and **10m** are efficient antiproliferative agents that may operate as EGFR inhibitors.

**3.2.4. HER-2 inhibitory assay.** An *in vitro* study was performed to evaluate the anti-HER-2 efficacy of derivatives **10c**, **10e**, **10k**, and **10m-o**. Lapatinib functioned as the standard medicine.<sup>45</sup> The findings are displayed in Table 2. The findings demonstrated that the analyzed compounds had potent HER-2 inhibitory activity, with  $\text{IC}_{50}$  values ranging from 29 to 43 nM, compared to the reference lapatinib, which had an  $\text{IC}_{50}$  value of 26 nM.

Again, compounds **10e** and **10k**, the most effective antiproliferative and EGFR inhibitors, displayed the highest potency as HER-2 inhibitors with  $\text{IC}_{50}$  values of  $29 \pm 1$  and  $31 \pm 2$  nM, indicating comparable efficacy to the reference lapatinib. Compounds **10c**, **10n**, and **10o** exhibited significant activity as HER-2 inhibitors, with  $\text{IC}_{50}$  values of 34, 39, and 37 nM, respectively, which is slightly less potent than compounds **10e** and **10k**, as well as the reference medication lapatinib. Eventually, compound **10m** was identified as the least effective derivative of HER-2 inhibitors, exhibiting an  $\text{IC}_{50}$  value of  $43 \pm 2$  nM, which is 1.7-fold less potent than lapatinib ( $\text{IC}_{50}$  value = 26 nM). These *in vitro* studies indicate that compounds **10c**, **10e**, and **10k** exhibit significant antiproliferative activity and may function as dual EGFR/HER-2 inhibitors.

Table 2  $\text{IC}_{50}$  values of compounds **10c**, **10e**, **10k**, **10m**, **10n** and **10o** against EGFR, HER-2, BRAF<sup>V600E</sup>, and VEGFR-2<sup>a</sup>

Compound	EGFR inhibition $\text{IC}_{50} \pm \text{SEM}$ (nM)	HER-2 inhibition $\text{IC}_{50} \pm \text{SEM}$ (nM)	BRAF <sup>V600E</sup> inhibition $\text{IC}_{50} \pm \text{SEM}$ (nM)	VEGFR-2 inhibition $\text{IC}_{50} \pm \text{SEM}$ (nM)
<b>10c</b>	$77 \pm 4$	$34 \pm 2$	$76 \pm 5$	$27 \pm 1$
<b>10e</b>	$73 \pm 4$	$31 \pm 2$	$69 \pm 5$	$20 \pm 1$
<b>10k</b>	$69 \pm 4$	$29 \pm 1$	$63 \pm 4$	$21 \pm 1$
<b>10m</b>	$87 \pm 5$	$43 \pm 2$	ND	ND
<b>10n</b>	$83 \pm 5$	$39 \pm 2$	ND	ND
<b>10o</b>	$79 \pm 4$	$37 \pm 2$	ND	ND
Erlotinib	$80 \pm 5$	ND	ND	ND
Lapatinib	ND	$26 \pm 1$	ND	ND
Vemurafenib	ND	ND	$30 \pm 3$	ND
Sorafenib	ND	ND	ND	$0.17 \pm 0.001$

<sup>a</sup> ND: Not Determined.



**3.2.5. BRAF<sup>V600E</sup> inhibitory assay.** An *in vitro* study assessed the potency of derivatives **10c**, **10e**, and **10k** as BRAF<sup>V600E</sup> inhibitors. Vemurafenib was used as a reference drug.<sup>55</sup> Table 2 summarizes the findings. The enzyme assay revealed that the evaluated compounds notably inhibited BRAF<sup>V600E</sup>, with IC<sub>50</sub> values between 63 and 76 nM. All analyzed derivatives have higher IC<sub>50</sub> values, indicating reduced potency compared to vemurafenib (IC<sub>50</sub> = 30 ± 3). Compounds **10k** and **10e** displayed the most pronounced inhibitory effect against BRAF<sup>V600E</sup> (IC<sub>50</sub> = 63 and 69 nM, respectively), indicating at least a 2-fold decreased potency relative to the reference vemurafenib. Compound **10c** had the lowest potency as a BRAF inhibitor, with an IC<sub>50</sub> value of 76 nM, rendering it 2.5-fold less efficient than vemurafenib. The study's findings indicate that the compounds **10k** and **10e** exhibit moderate anti-BRAF<sup>V600E</sup> activity, requiring structural modifications to enhance their efficacy against BRAF.

**3.2.6. VEGFR-2 inhibitory assay.** The inhibitory effects of compounds **10c**, **10e**, and **10k** on VEGFR-2 were evaluated by kinase assays, with sorafenib as the control drug.<sup>21</sup> Table 2 displays the results as IC<sub>50</sub> values. The results indicated that the examined compounds significantly inhibited VEGFR-2, exhibiting IC<sub>50</sub> values between 21 and 27 nM, compared to sorafenib, which demonstrated an IC<sub>50</sub> of 0.17 nM. In every case, the compounds examined exhibited lower potency than sorafenib as VEGFR-2 inhibitors, although displayed more potency than EGFR and HER-2 inhibitors. Compounds **10k** and **10e**, identified as the most effective antiproliferative, EGFR, and HER-2 inhibitors, had substantial activity as VEGFR-2 inhibitors with IC<sub>50</sub> values of 21 and 20 nM, indicating their potential as multi-kinase EGFR/HER-2/VEGFR-2 inhibitors.

### 3.3. Apoptotic markers assays

Apoptosis, or programmed cell death, is regarded as a crucial mechanism for the elimination of undesirable cells by the body.<sup>60</sup> Consequently, inducing apoptosis in cancer cells will result in their inevitable demise and enhance the alleviation of cancer proliferation. A comprehensive understanding of apoptosis elucidates that it is influenced by the expression of caspases and Bcl-2 family proteins, which encompass both anti-apoptotic and pro-apoptotic members.<sup>61</sup> The induction of apoptosis is regarded as one of the most effective approaches for targeting cancer.

Compounds **10e** and **10k** were assessed for their capacity to induce apoptosis in MCF-7 breast cancer cells by examining the expression of crucial apoptotic markers, namely Bcl-2, p53, and Bax. The findings are presented in Table 3. The Bcl-2 protein family, consisting of pro-apoptotic proteins (Bax) and anti-

apoptotic proteins (Bcl-2), predominantly governs apoptosis. We examined the concentrations of Bcl-2 and Bax proteins in MCF7 breast cancer cells subjected to treatment with compounds **10e** and **10k**. Results indicate a significant 9-fold elevation in Bax levels and a 4.5-fold reduction in Bcl-2 levels for **10k** compared to the control untreated cells. Furthermore, compound **10e** exhibited a notable 8.6-fold elevation in Bax levels and a three-fold reduction in Bcl-2 levels. These observations suggest that apoptosis may play a role in the anti-proliferative activities of the investigated compounds.

The capacity for p53 overexpression to trigger apoptosis may clarify the common inactivation of p53 enzymes by cancer cells during transformation. The p53 levels in cancer cells subjected to compounds **10e** and **10k** exhibited a substantial increase, surpassing those of the untreated control cells by a minimum of 5-fold. This observation indicates that greater levels of the p53 protein may govern the apoptotic process in these new compounds.

### 3.4. Docking studies

**3.4.1. Docking into EGFR active site.** In this study, molecular docking was performed to investigate the interactions of selected compounds (**10k**, **10e**, and **10h**) with the active site of the epidermal growth factor receptor (EGFR). The EGFR structure used for docking was retrieved from the Protein Data Bank (PDB ID: 1M17),<sup>62</sup> where the co-crystallized ligand, erlotinib, served as a reference. Docking was performed using Autodock Vina,<sup>63,64</sup> a widely used software for predicting protein-ligand binding poses and affinities. The docking results were then visualized using Discovery Studio Visualizer, which enabled a detailed examination of the ligand-receptor interactions.

First, the docking procedure was validated by redocking erlotinib into the EGFR active site, comparing the predicted binding pose and affinity with the experimental values obtained from the crystal structure. The redocking results revealed a binding affinity of  $-9.4 \text{ kcal mol}^{-1}$  and an RMSD of  $1.4429 \text{ \AA}$  when compared to the original co-crystallized structure as shown in Fig. 5. The RMSD value of less than  $2.0 \text{ \AA}$  confirmed that the docking protocol accurately reproduced the ligand's binding pose, ensuring the reliability and precision of the

**Table 3** Outcomes of apoptotic experiments for **10e** and **10k** against Bax, p53, and Bcl2

Compound no.	Bcl-2 (ng mL <sup>-1</sup> )	Bax (pg mL <sup>-1</sup> )	p53 (pg mL <sup>-1</sup> )
<b>10e</b>	$1.30 \pm 0.001$	$520 \pm 3$	$360 \pm 2$
<b>10k</b>	$1.10 \pm 0.001$	$550 \pm 3$	$385 \pm 2$
Control MCF-7 cell	5	60	65

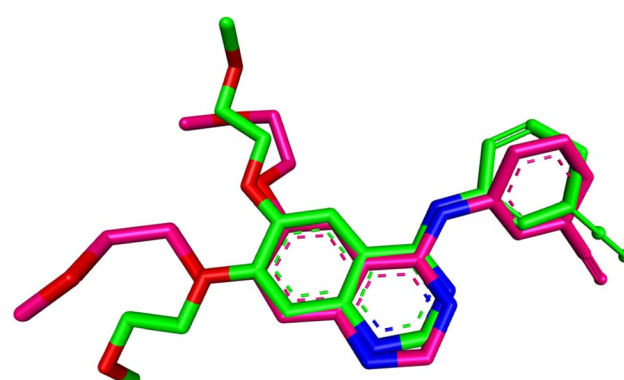


**Fig. 5** Superimposition of redocked (green) and co-crystallized (magenta) poses of erlotinib in the EGFR active site (RMSD =  $1.4429 \text{ \AA}$ ).



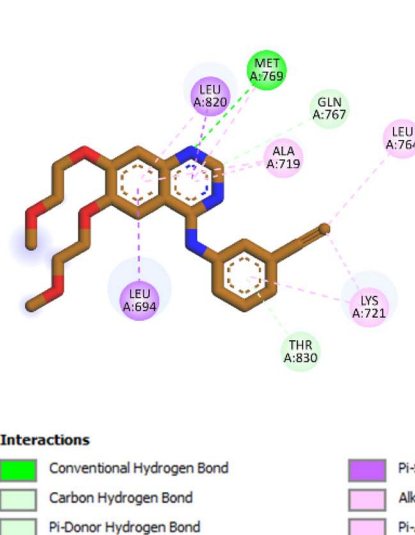
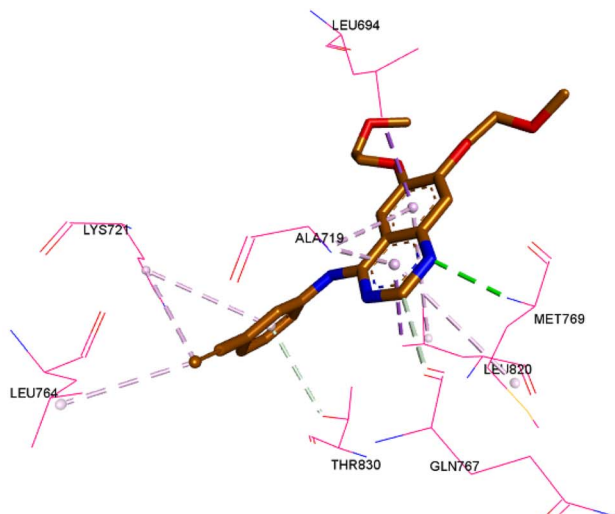
**A****B**

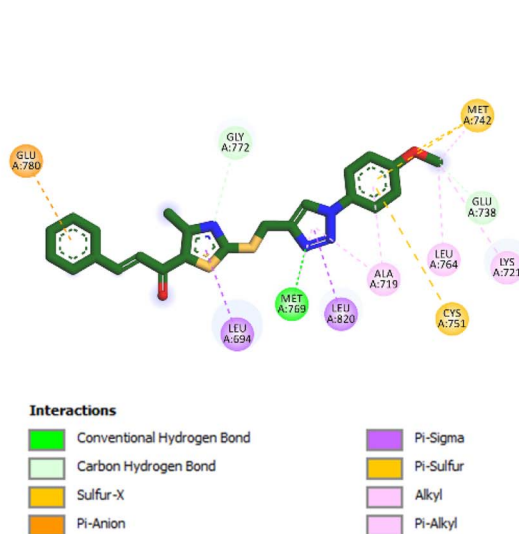
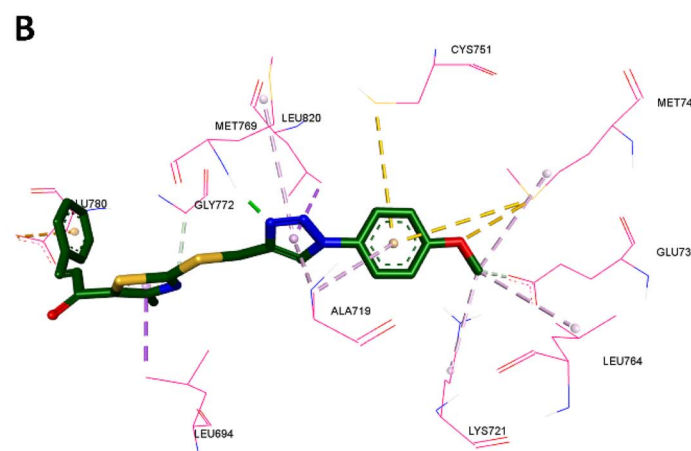
Fig. 6 2D (A) and 3D (B) interactions of erlotinib within the EGFR active site.

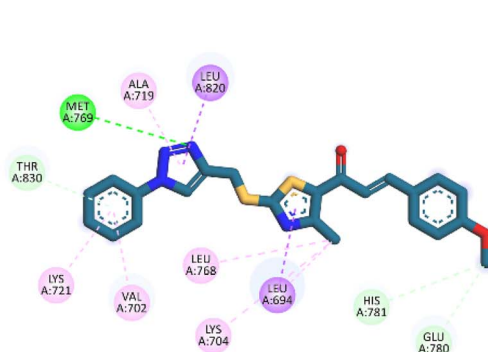
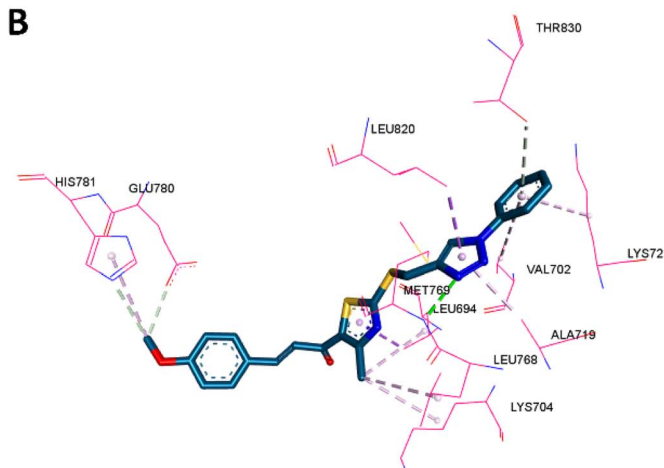
method. With this validation in place, the docking procedure was applied to the compounds of interest: **10k**, **10e**, and **10h**.

For compound **10k** (Fig. 7), the 1,2,3-triazole group formed a classical hydrogen bond with Met769, an interaction similar to that made by erlotinib's quinazoline ring (Fig. 6), which is critical for EGFR binding. The triazole ring of **10k** also established hydrophobic interactions with Ala719 and Leu820, mirroring those of erlotinib with these residues. In addition, the benzene rings in **10k** engaged in Pi-sulfur interactions with Cys751 and Met742, which were absent in erlotinib. The thiazole ring contributed to Pi-sigma interactions with Leu694, a feature shared with erlotinib. Notably, the methoxy group on the benzene ring of **10k** made significant contributions by forming hydrophobic interactions with Leu764 and Lys721, similar to the interactions of the ethynyl group in erlotinib with these residues. Moreover, the methoxy group in **10k** uniquely

formed a non-classical hydrogen bond with Glu738, which erlotinib lacks. These distinctive interactions, including the Pi-sulfur contacts and additional hydrogen bonds with Glu738 and Gly772, enhance the binding affinity of **10k**, accounting for its superior potency compared to erlotinib.

In the case of compound **10e** (Fig. 8), the 1,2,3-triazole group formed a classical hydrogen bond with Met769, mimicking the essential role of erlotinib's quinazoline ring in EGFR inhibition. Like **10k**, the triazole ring in **10e** displayed hydrophobic interactions with Ala719 and Leu820, similar to those made by erlotinib's quinazoline ring. The thiazole ring of **10e** showed Pi-sigma interactions with Leu694, a conserved feature also observed in erlotinib. Importantly, the methoxy group in **10e** played a critical role by forming non-classical hydrogen bonds with His781 and Glu780, interactions absent in erlotinib, underscoring the significance of the methoxy group in

**A****B**Fig. 7 2D (A) and 3D (B) interactions of **10k** within the EGFR active site.

**A****B**Fig. 8 2D (A) and 3D (B) interactions of **10e** within the EGFR active site.

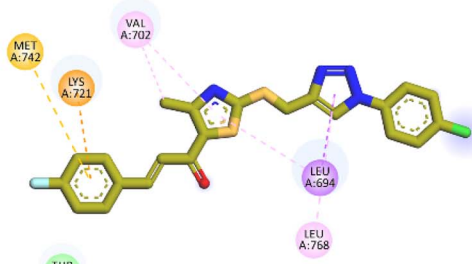
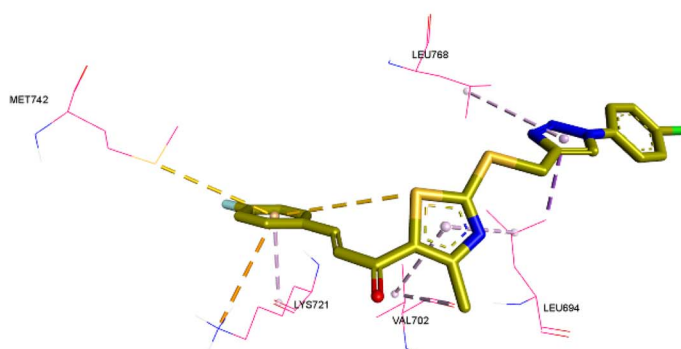
enhancing binding. Additionally, **10e** formed a non-classical (Pi-donor) hydrogen bond with Thr830, a novel interaction not observed in erlotinib. These unique contributions, particularly the hydrogen bond with Thr830 and the stabilizing interactions involving the methoxy group with His781 and Glu780, likely account for **10e**'s improved potency relative to erlotinib. However, it remains slightly less potent than **10k**.

Moving to compound **10h** (Fig. 9), the 1,2,3-triazole group exhibited hydrophobic (Pi-sigma) interactions with Leu694, similar to the interactions of erlotinib's quinazoline ring with the same residue. However, unlike **10k** and **10e**, **10h** adopted a distinct binding pose that prevented its triazole ring from forming the crucial hydrogen bond with Met769, an interaction vital for binding and present in erlotinib and the more potent compounds. The absence of this key interaction likely contributes to **10h**'s lower potency. Furthermore, the lack of

a stabilizing methoxy group, which was replaced by chloro and fluoro groups that failed to engage in significant interactions, further weakened **10h**'s binding affinity, resulting in reduced activity compared to the other compounds.

**3.4.2. Docking into HER-2 active site.** To validate the docking procedure for HER-2, the co-crystallized ligand TAK-285 (ref. 65) was redocked into the HER-2 active site. The redocking results yielded an RMSD of 1.0845 Å and a binding affinity of  $-8.3$  kcal mol $^{-1}$ , indicating that the docking protocol accurately reproduced the ligand's binding pose and affinity. This validation confirms the reliability of the method for docking compounds into the HER-2 active site. The superimposition of the redocked TAK-285 and the co-crystallized pose is shown in Fig. 10.

In addition to validating the docking procedure, we also docked compound **10k**, which demonstrated the best binding

**A****B**Fig. 9 2D (A) and 3D (B) interactions of **10h** within the EGFR active site.

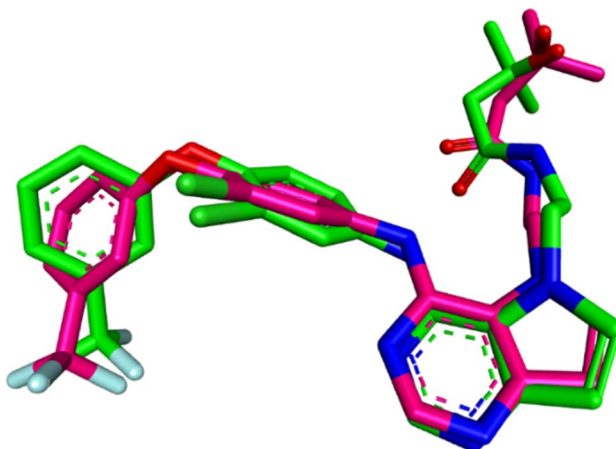


Fig. 10 Superimposition of redocked (green) and co-crystallized (magenta) poses of TAK-285 in the HER-2 active site (RMSD = 1.0845 Å).

profile in HER-2, alongside the reference compound lapatinib. The docking results revealed binding affinities of  $-8.8$  kcal mol $^{-1}$  for **10k** and  $-9.2$  kcal mol $^{-1}$  for lapatinib, suggesting comparable binding strengths. *In vitro* assays also confirmed that the HER-2 inhibition activity of **10k** was similar to that of lapatinib, supporting the docking predictions.

Several interactions between compound **10k** and HER-2 were found to be similar to those with lapatinib. Specifically, the nitrogen atom of the 1,2,3-triazole moiety of compound **10k** establishes a hydrogen bond with Met801, paralleling the interaction between the nitrogen atom of lapatinib's quinazoline ring and the same residue, which is crucial for HER-2 suppression. Furthermore, the triazole ring of **10k** forms hydrophobic interactions with Val734 and Ala751, similar to the hydrophobic interactions established by the quinazoline ring of lapatinib with these residues. The benzene ring of **10k** also

participates in hydrophobic interactions with Leu796, similar to those observed with the benzene ring of lapatinib.

The thiazole ring of **10k** forms hydrophobic contacts with Lys753, a feature also observed with lapatinib's benzene ring. Furthermore, compound **10k** forms an additional characteristic hydrogen bond with Lys753, an interaction that is not present in lapatinib, which could further stabilize its binding. Notably, the benzene ring of **10k** also engages in a unique pi-pi T-shaped interaction with Phe1004, a feature absent in lapatinib. The methoxy group of **10k** forms additional hydrophobic interactions with Cys805, further distinguishing it from lapatinib. The 2D and 3D interactions of lapatinib within the HER-2 active site are depicted in Fig. 11, while the corresponding interactions of compound **10k** are shown in Fig. 12.

Following the EGFR and HER-2 docking analyses, compounds **10k** and **10e** were further evaluated for their binding to VEGFR-2 (PDB ID: 3U6J),<sup>66</sup> given their promising VEGFR-2 inhibition observed *in vitro*. The docking scores indicated strong binding affinities of  $-9.30$  kcal mol $^{-1}$  for **10k** and  $-9.34$  kcal mol $^{-1}$  for **10e**, compared to  $-10.15$  kcal mol $^{-1}$  for the reference inhibitor sorafenib.

For **10k**, several interactions were conserved with those observed in sorafenib, including hydrophobic contacts with Leu889, Val848, Leu1035, and Ala866, as well as hydrogen bonding with Lys868. These collaborative interactions demonstrate a comparable binding orientation inside the VEGFR-2 active region and align with its documented *in vitro* efficacy. In addition, **10k** established unique interactions do not present in sorafenib, including an electrostatic interaction with Glu885 *via* the thiazole nitrogen, and C-H bonding with Cys919 through its methoxy group, whereas sorafenib forms a classical H-bond at this position. Moreover, **10k** formed additional hydrophobic contacts with Val898 and Ile1044, residues not engaged by sorafenib. These added interactions likely enhance ligand stabilization and correlate well with its strong VEGFR-2 inhibition in biological assays. Visual summaries of the

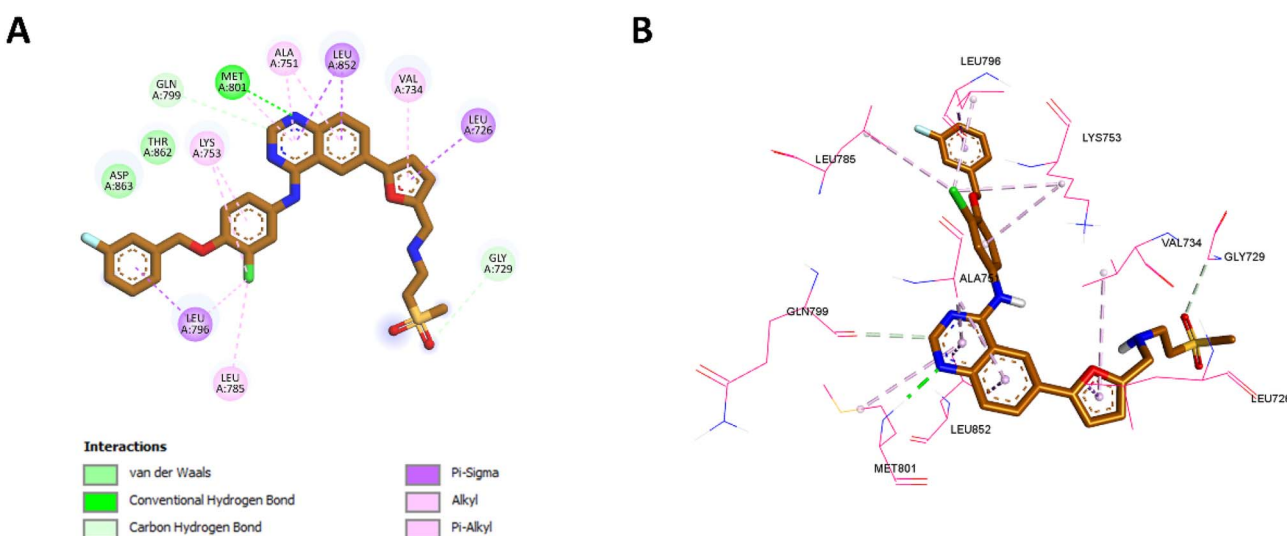
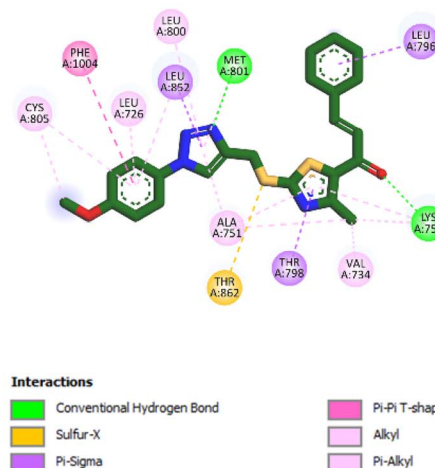


Fig. 11 2D (A) and 3D (B) interactions of lapatinib within the HER-2 active site.



A



B

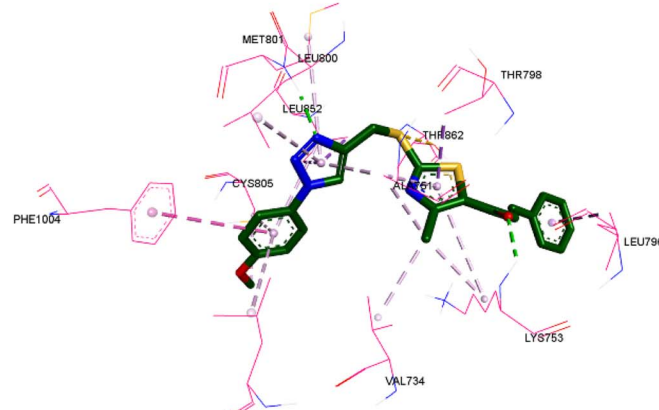


Fig. 12 2D (A) and 3D (B) interactions of 10k within the HER-2 active site.

interactions exhibited by sorafenib and 10k are presented in Fig. 13 and 14, respectively.

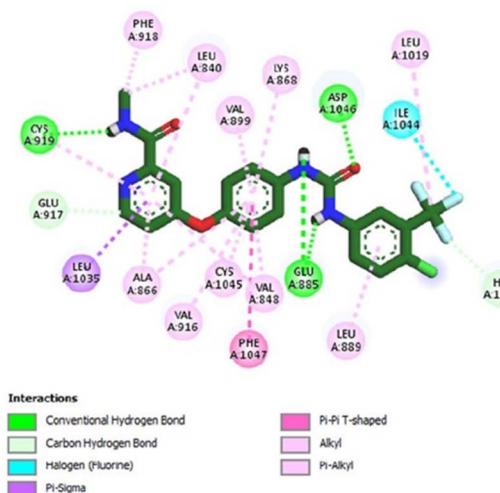
Similarly, **10e** retained multiple conserved interactions, such as hydrogen bonding with Lys868 and hydrophobic contacts with Leu889, Val848, Leu1035, and Ala866, aligning with its binding orientation relative to sorafenib. However, **10e** also introduced novel interactions, including hydrophobic engagement with Cys919 and Val914, and unique contacts involving its methoxy and thiazole moieties. Notably, unlike **10k**, **10e** did not interact with Val898 or Ile1044, which may account for its slightly reduced potency *in vitro* despite a marginally higher docking score. These interactions are illustrated in Fig. 15.

**3.4.3. ADME prediction.** The physicochemical and pharmacokinetic properties of compounds **10k** and **10e** were calculated using the SwissADME tool,<sup>67,68</sup> which provides a comprehensive analysis of drug-likeness, solubility, lipophilicity, and absorption characteristics based on molecular

structure. Both compounds have identical molecular formulas ( $C_{23}H_{20}N_4O_2S_2$ ) and molecular weights (448.56 g mol<sup>-1</sup>), indicating similar molecular sizes and structures, which could contribute to their comparable pharmacological behavior. As shown in Fig. 16, the bioavailability radar plots for compounds **10k** and **10e** reflect their promising physicochemical profiles. Both compounds exhibit moderate lipophilicity, solubility, and polarity, suggesting they are well-suited for membrane permeability and targeted delivery to specific tissues or cells. The radar plots indicate that both compounds fall within acceptable ranges for most pharmacokinetic parameters, with moderate potential for oral bioavailability.

Both compounds exhibit moderate lipophilicity. Specifically, compound **10k** has a calculated  $\log P$  of 4.54, while compound **10e** shows a very similar value of 4.52. This close similarity in lipophilicity suggests that both compounds are likely to display comparable membrane permeability and distribution behavior

A



B

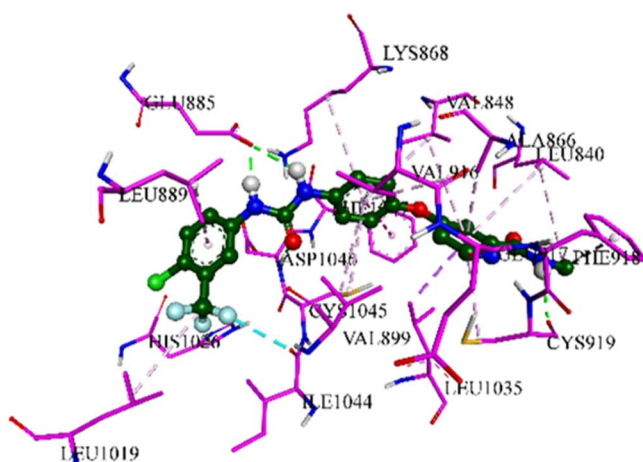


Fig. 13 2D (A) and 3D (B) interactions of sorafenib within the VEGFR-2 active site.



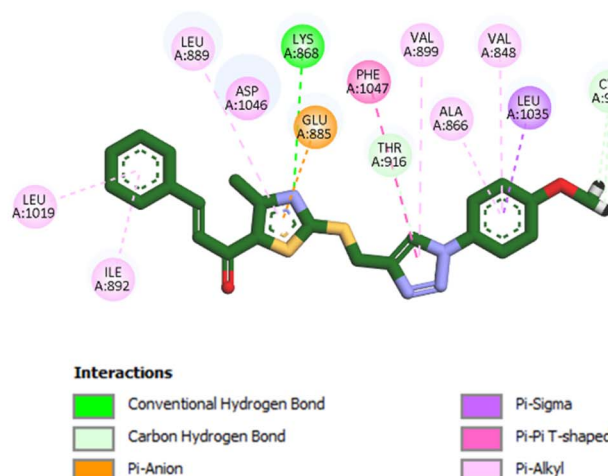
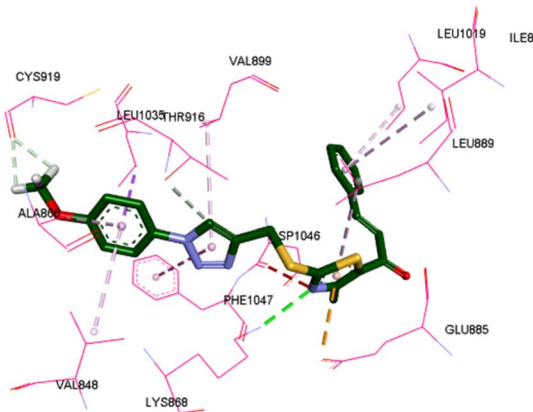
**A****B**

Fig. 14 2D (A) and 3D (B) interactions of 10k within the VEGFR-2 active site.

*in vivo*. Such log *P* values are within the range generally associated with effective cell membrane penetration, supporting their potential for efficient target engagement, particularly in hydrophobic binding pockets of EGFR and HER-2. However, it is worth noting that the compounds exhibit low gastrointestinal (GI) absorption. This is typically considered a disadvantage, but in the context of these compounds, it might be useful. Low GI absorption could limit systemic exposure and potential off-target effects, thereby increasing specificity for the targeted cancer cells. Moreover, compounds with low absorption may sometimes be more effective at localizing to specific tissues, such as tumors, where the drug may accumulate in higher concentrations.

The water solubility results show that both compounds are moderately soluble according to the ESOL model but poorly

soluble in the Ali and SILICOS-IT models. While poor solubility can pose challenges to oral bioavailability, it can be leveraged in drug delivery systems that enhance solubility, such as nanoparticles or liposomes, thereby mitigating this issue.

Both compounds demonstrate a bioavailability score of 0.55, indicating moderate potential for oral bioavailability. Furthermore, the compounds do not violate Lipinski's Rule of Five, indicating that they are likely to have favorable pharmacokinetic profiles in terms of absorption, distribution, metabolism, and excretion (ADME). However, both compounds violate Muegge's rule due to an XLOGP3 greater than 5, which suggests that they may exhibit some degree of poor solubility or permeability, aligning with their GI absorption and solubility profiles.

Regarding their interaction with drug-metabolizing enzymes, both compounds inhibit several cytochrome P450 enzymes, such

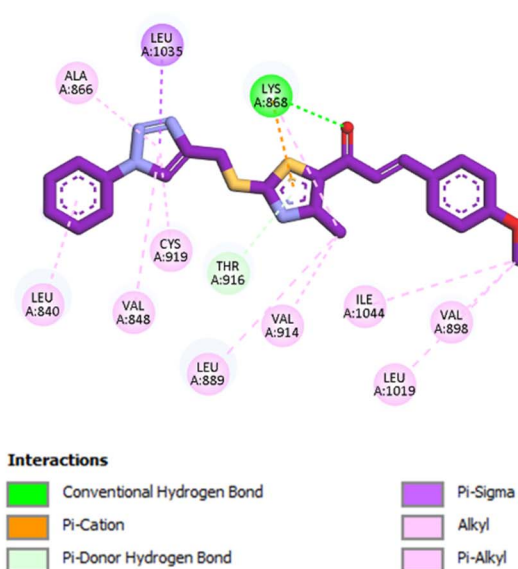
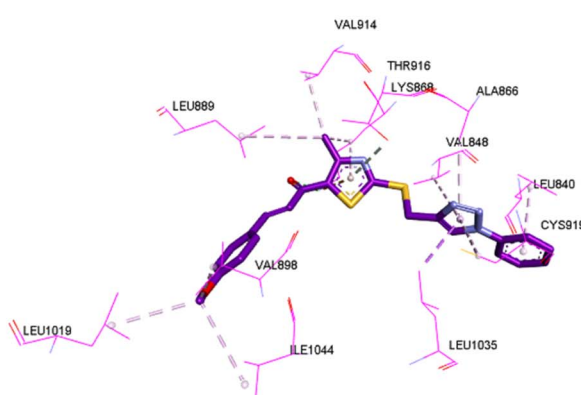
**A****B**

Fig. 15 2D (A) and 3D (B) interactions of 10e within the VEGFR-2 active site.



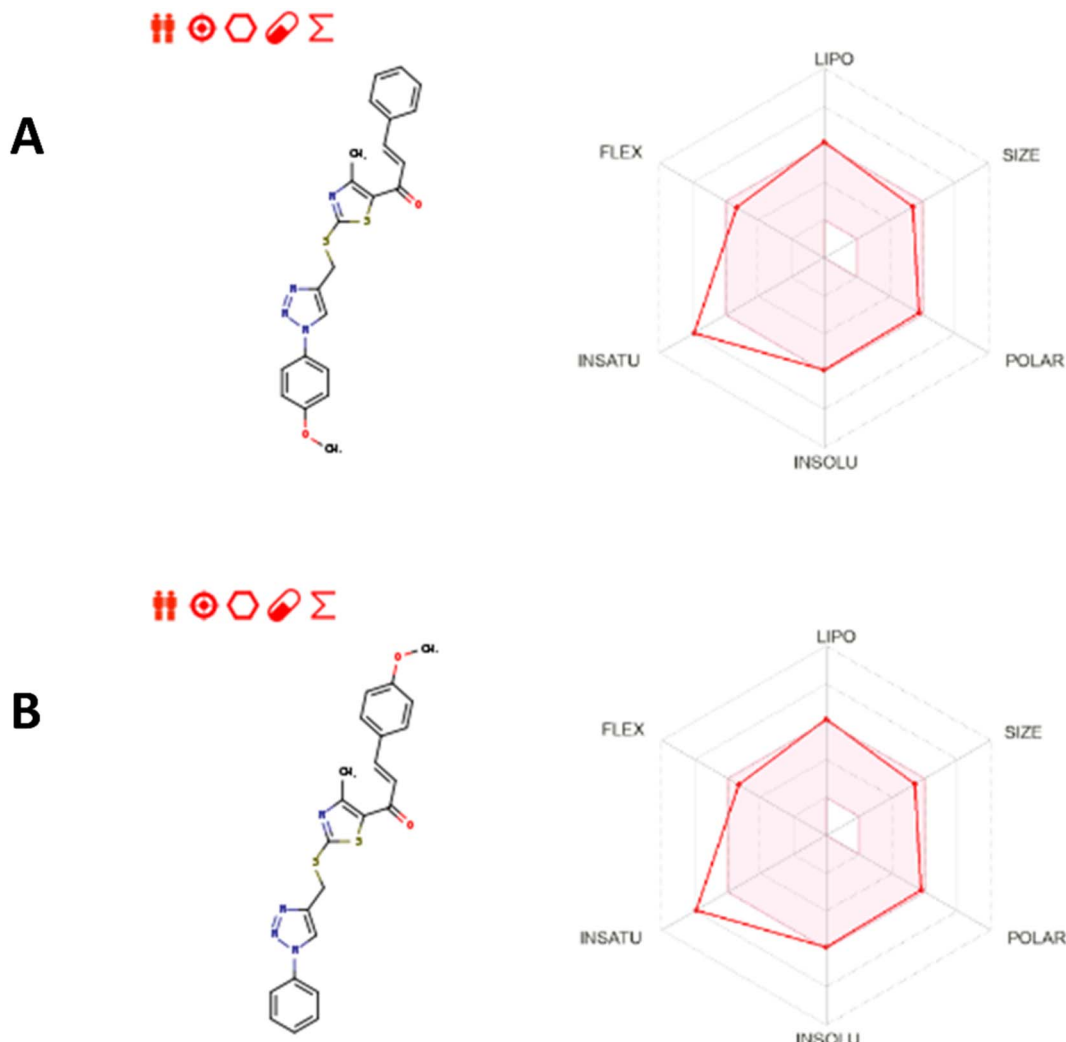


Fig. 16 (a) Bioavailability radar plot of compound **10k**; (b) bioavailability radar plot of compound **10e**.

as CYP2C19, CYP2C9, and CYP3A4. These interactions could affect the metabolism of co-administered drugs, which may be a consideration in combination therapies. However, the lack of inhibition of other P450 enzymes and transporters, such as P-glycoprotein (P-gp), suggests that these compounds may have a relatively safe metabolic profile compared to other drugs that interact more broadly with these systems.

Additionally, both compounds are free from PAINS (pan-assay interference compounds) alerts, which is a positive indicator of their chemical quality. Although both compounds exhibit lead-likeness violation due to their molecular weight and rotatable bonds, they are still considered synthetically accessible with ease (accessibility scores close to 4), suggesting that they could be further developed into drug candidates with practical synthesis routes.

Given that compounds **10k** and **10e** have already been demonstrated to effectively target the EGFR and HER-2 pathways through *in vitro* assays, their physicochemical and pharmacokinetic properties further strengthen their potential as promising candidates for therapeutic development. Their lipophilicity and moderate bioavailability suggest they are well-suited for targeting

specific tissues or cells, including those expressing EGFR and HER-2, making them effective in treating cancers driven by these pathways.

### 3.5. Structure-activity relationship analysis (SAR analysis)

The following points can be noted regarding the SAR of novel compounds **10a–o**:

(1) The 1,2,3-triazole moiety is crucial for EGFR inhibitory activity, as it establishes a hydrogen bond with Met769, similar to the contact formed by erlotinib's quinazoline ring, which is vital for EGFR binding.

(2) Regarding HER-2 activity, the nitrogen atom of the 1,2,3-triazole moiety forms a hydrogen bond with Met801, analogous to the interaction between the nitrogen atom of lapatinib's quinazoline ring and the same residue, which is essential for HER-2 inhibition.

(3) The thiazole ring establishes a hydrogen bond with Lys868, which is crucial for the suppression of VEGFR-2 activity.

(4) Furthermore, the phenyl group of the 1,2,3-triazole moiety participated in several hydrophobic interactions within



the EGFR, VEGFR-2, and HER-2 sites, thereby enhancing binding to the active sites of these enzymes and thereby increasing activity.

(5) The substitution pattern at the *para* position of the phenyl group in the 1,2,3-triazole moiety ( $R_2$ ) significantly influences activity, with the methoxy group being the most favored due to hydrophobic interactions with Leu764 and Lys721, analogous to the ethynyl group interactions of erlotinib with these residues or with Cys805 in the HER-2 active site. The methoxy group formed a significant hydrogen bond with Cys919 in VEGFR-2 active site.

(6) The thiazole ring facilitated Pi-sigma interactions with Leu694, a characteristic also present in erlotinib.

(7) The carbonyl oxygen of the chalcone moiety establishes a hydrogen bond with Lys753, an interaction absent in lapatinib, which may further strengthen the binding within the HER-2 active site.

## 4. Conclusion

Compounds **10c**, **10e**, **10k**, **10m**, **10n**, and **10o** demonstrated remarkable antiproliferative efficacy and a favorable safety profile, making them the most active hybrids in this experiment. The MTT antiproliferative experiment revealed that MCF-7 breast cancer cells were the most appropriate targets for these agents. Compounds **10e** and **10k** have the highest anti-breast cancer activity, with  $IC_{50}$  values of 24 and 21 nM against the MCF-7 cell line, respectively. Notably, they exhibited the highest efficacy as multi-kinase EGFR/HER-2/VEGFR-2 inhibitors, while demonstrating moderate anti-BRAF<sup>V600E</sup> action. In molecular modeling studies, compounds **10e** and **10k** exhibited significant binding affinity for the crucial amino acids Met769, Glu738, Leu764, and Lys721 in the EGFR kinase active site, as well as Met801 in the HER-2 kinase pocket. Additionally, their binding modes within the VEGFR-2 active site involved key residues such as Lys868, Glu885, and Cys919, further supporting their VEGFR-2 inhibition profile. Moreover, the active compounds conformed to Lipinski's rule of five, exhibiting satisfactory ADMET data that demonstrated their potential for subsequent stages of drug discovery. The active chemicals and their biological effects, along with modeling studies, may serve as prototypes for future research and development. Further research is needed to determine their *in vivo* efficacy and toxicity. Future studies will focus on enhancing BRAF<sup>V600E</sup> inhibition while maintaining the compounds' anticancer properties. Also, we will empirically ascertain the log  $P$  values along with other physicochemical parameters for a representative subset of compounds and compare them with the calculated values.

## Conflicts of interest

The authors stated there were no potential conflicts of interest.

## Data availability

The authors assert that any data supporting this study can be found in the supplementary information (SI). Supplementary

information is available. See DOI: <https://doi.org/10.1039/d5ra07556d>.

## Acknowledgements

The authors acknowledge support from the KIT-Publication Fund of the Karlsruhe Institute of Technology.

## References

- 1 J. H. Choi and J. Y. Ro, *Adv. Anat. Pathol.*, 2021, **28**, 44–58.
- 2 M. Vaduganathan, G. A. Mensah, J. V. Turco, V. Fuster and G. A. Roth, *J. Am. Coll. Cardiol.*, 2022, **80**, 2361–2371.
- 3 K. Hacker, *Mayo Clin. Proc.: Innov. Qual. Outcomes*, 2024, **8**, 112–119.
- 4 B. Zou, P. Wu, J. Chen, J. Luo, Y. Lei, Q. Luo, B. Zhu and M. Zhou, *BMC Cancer*, 2025, **25**, 503.
- 5 L. H. Al-Wahaibi, H. A. Abou-Zied, M. H. Abdelrahman, M. M. Morcoss, L. Trembleau, B. G. Youssif and S. Bräse, *Front. Chem.*, 2024, **12**, 1432920.
- 6 L. H. Al-Wahaibi, M. A. Elbastawesy, N. E. Aboda, B. G. Youssif, S. Bräse, S. N. Shabaan, G. H. Sayed and K. E. Anwer, *Pharmaceuticals*, 2024, **17**, 1284.
- 7 L. H. Al-Wahaibi, A. M. Elshamsy, T. F. Ali, B. G. Youssif, S. Bräse, M. Abdel-Aziz and N. A. El-Koussi, *ACS Omega*, 2024, **9**, 34358–34369.
- 8 Y. Zhou, Z. Yao, Y. Lin and H. Zhang, *Pharmaceutics*, 2024, **16**, 888.
- 9 N. Zehra, Z. Uddin, M. I. A. Zada and M. Ikram, in *Cell Signaling*, CRC Press, 2025, pp. 231–267.
- 10 Y. Sun, F. A. Dinenno, P. Tang and M. I. Kontaridis, *Front. Cardiovasc. Med.*, 2024, **11**, 1445739.
- 11 A. Levitzki, *Bioorganic Chemistry of Biological Signal Transduction*, 2001, pp. 1–15.
- 12 E. Acosta-Ramos, M. Segovia-Mendoza and J. A. Olivares-Reyes, *Breast Cancer Treatment: an Interdisciplinary Approach*, 2024, vol. 7, p. 237.
- 13 S. Hao, J.-h. Wang, L. Hou, J.-w. Liang, J.-h. Yan, Y.-f. Niu, X.-y. Li, Q. Sun and F.-h. Meng, *Bioorg. Chem.*, 2024, **151**, 107686.
- 14 Y. Yang, Y. Mou, L. X. Wan, S. Zhu, G. Wang, H. Gao and B. Liu, *Med. Res. Rev.*, 2024, **44**, 2600–2623.
- 15 M. Puzzo, M. De Santo, C. Morelli, A. Leggio and L. Pasqua, *Small Sci.*, 2024, **4**, 2400113.
- 16 C. Grobbelaar, V. Steenkamp and P. Mabeta, *Curr. Issues Mol. Biol.*, 2025, **47**, 179.
- 17 A. □andor, O. Crişan, G. Marc, I. Fizeşan, I. Ionuţ, C. Moldovan, A. Stana, I. Oniga, A. Pírnau and L. Vlase, *Pharmaceutics*, 2025, **17**, 260.
- 18 A. Zabihi, *Int. J. Biol. Macromol.*, 2025, 143838.
- 19 Y. Zhang, J. Li, L. Zhang and Y. Zhang, *Expert Rev. Clin. Immunol.*, 2025, **21**(5), 577–586.
- 20 T. Xia, J. Yu, M. Du, X. Chen, C. Wang and R. Li, *MedComm*, 2025, **6**, e70057.
- 21 M. A. Mahmoud, A. F. Mohammed, O. I. Salem, S. M. Rabea and B. G. Youssif, *J. Mol. Struct.*, 2023, **1282**, 135165.



22 W. E. Elgammal, H. Elkady, M. A. Dahab, H. A. Mahdy, M. Hagraas, A. Nofal, B. A. Alsfouk, E. B. Elkaeed, I. H. Eissa and A. M. Metwaly, *Future Med. Chem.*, 2025, 1–13.

23 A. A. Marzouk, S. A. Abdel-Aziz, K. S. Abdelrahman, A. S. Wanas, A. M. Gouda, B. G. Youssif and M. Abdel-Aziz, *Bioorg. Chem.*, 2020, **102**, 104090.

24 M. D. Ansari, Nouman, R. Mehandi, M. Rana and Rahisuddin, *Advances in Antifungal Drug Development: Natural Products with Antifungal Potential*, 2024, pp. 535–563.

25 L. H. Al-Wahaibi, M. H. Abdel-Rahman, K. El-Adl, B. G. Youssif, S. Bräse and S. A. Abdel-Aziz, *ACS Omega*, 2024, **9**, 33494–33509.

26 S. Gcharge and S. Alegaon, *Chem. Biodiversity*, 2024, **21**, e202301738.

27 A. Petrou, M. Fesatidou and A. Geronikaki, *Molecules*, 2021, **26**, 3166.

28 A. H. Abdelazeem, M. T. El-Saadi, E. G. Said, B. G. Youssif, H. A. Omar and S. M. El-Moghazy, *Bioorg. Chem.*, 2017, **75**, 127–138.

29 S. A. Abdel-Aziz, E. S. Taher, P. Lan, G. F. Asaad, H. A. Gomaa, N. A. El-Koussi and B. G. Youssif, *Bioorg. Chem.*, 2021, **111**, 104890.

30 M. Lindauer and A. Hochhaus, *Small Molecules in Hematology*, 2018, pp. 29–68.

31 A. Puszkiel, G. Noé, A. Bellesoeur, N. Kramkimel, M.-N. Paludetto, A. Thomas-Schoemann, M. Vidal, F. Goldwasser, E. Chatelut and B. Blanchet, *Clin. Pharmacokinet.*, 2019, **58**, 451–467.

32 J. Koehnke, A. F. Bent, W. E. Houssen, G. Mann, M. Jaspars and J. H. Naismith, *Curr. Opin. Struct. Biol.*, 2014, **29**, 112–121.

33 P.-C. Lv, C.-F. Zhou, J. Chen, P.-G. Liu, K.-R. Wang, W.-J. Mao, H.-Q. Li, Y. Yang, J. Xiong and H.-L. Zhu, *Bioorg. Med. Chem.*, 2010, **18**, 314–319.

34 M. A. Sabry, M. A. Ghaly, A. R. Maarouf and H. I. El-Subbagh, *Eur. J. Med. Chem.*, 2022, **241**, 114661.

35 E. M. El-Sheref, S. Bräse, H. N. Tawfeek, F. A. Alasmary and B. G. Youssif, *Int. J. Mol. Sci.*, 2023, **24**, 13300.

36 E. M. El-Sheref, M. A. Elbastawesy, A. B. Brown, A. M. Shawky, H. A. Gomaa, S. Bräse and B. G. Youssif, *Molecules*, 2021, **26**, 6798.

37 M. Maghraby, O. Salem, B. Youssif and M. Sheha, *Chemical Biology & Drug Design*, 2022.

38 M. T. Maghraby, T. Mazyad Almutairi, S. Bräse, O. I. Salem, B. G. Youssif and M. M. Sheha, *Molecules*, 2023, **28**, 7092.

39 M. A. Mahmoud, A. F. Mohammed, O. I. Salem, T. M. Almutairi, S. Bräse and B. G. Youssif, *J. Enzyme Inhib. Med. Chem.*, 2024, **39**, 2305856.

40 G.-F. Zha, H.-L. Qin, B. G. Youssif, M. W. Amjad, M. A. G. Raja, A. H. Abdelazeem and S. N. A. Bukhari, *Eur. J. Med. Chem.*, 2017, **135**, 34–48.

41 H. A. Gomaa, M. E. Shaker, S. I. Alzarea, O. Hendawy, F. A. Mohamed, A. M. Gouda, A. T. Ali, M. M. Morcoss, M. H. Abdelrahman and L. Trembleau, *Bioorg. Chem.*, 2022, **120**, 105616.

42 A. M. Mohassab, H. A. Hassan, H. A. Abou-Zied, M. Fujita, M. Otsuka, H. A. Gomaa, B. G. Youssif and M. Abdel-Aziz, *J. Mol. Struct.*, 2024, **1297**, 136953.

43 H. N. Tawfeek, A. A. Hassan, S. Bräse, M. Nieger, Y. A. Mostafa, H. A. Gomaa, B. G. Youssif and E. M. El-Shreef, *Arab. J. Chem.*, 2022, **15**, 104280.

44 F. F. Hagar, S. H. Abbas, H. A. Gomaa, B. G. Youssif, A. M. Sayed, D. Abdelhamid and M. Abdel-Aziz, *BMC Chem.*, 2023, **17**, 116.

45 L. H. Al-Wahaibi, E. M. El-Sheref, H. N. Tawfeek, H. A. Abou-Zied, S. M. Rabea, S. Bräse and B. G. Youssif, *RSC Adv.*, 2024, **14**, 32978–32991.

46 T. Constantinescu and C. N. Lungu, *Int. J. Mol. Sci.*, 2021, **22**, 11306.

47 Y. Ouyang, J. Li, X. Chen, X. Fu, S. Sun and Q. Wu, *Biomolecules*, 2021, **11**, 894.

48 E. Praveenkumar, N. Gurrapu, P. K. Kolluri, N. Subhashini and A. Dokala, *Bioorg. Chem.*, 2021, **116**, 105377.

49 H. A. El-Sherief, B. G. Youssif, A. H. Abdelazeem, M. Abdel-Aziz and H. M. Abdel-Rahman, *Anti-Cancer Agents Med. Chem.*, 2019, **19**, 697–706.

50 F. F. Hagar, S. H. Abbas, D. Abdelhamid, H. A. Gomaa, B. G. Youssif and M. Abdel-Aziz, *Arch. Pharmazie*, 2023, **356**, 2200357.

51 L. H. Al-Wahaibi, M. A. Mahmoud, Y. A. Mostafa, A. E. Raslan and B. G. Youssif, *J. Enzyme Inhib. Med. Chem.*, 2023, **38**, 376–386.

52 A. A. Aly, M. B. Alshammari, A. Ahmad, H. A. Gomaa, B. G. Youssif, S. Braese, M. A. Ibrahim and A. H. Mohamed, *Arab. J. Chem.*, 2023, **16**, 104612.

53 M. A. Mahmoud, A. F. Mohammed, O. I. Salem, H. A. Gomaa and B. G. Youssif, *Arch. Pharmazie*, 2022, **355**, 2200009.

54 M. Hisham, H. A. Hassan, H. A. Gomaa, B. G. Youssif, A. M. Hayallah and M. Abdel-Aziz, *J. Mol. Struct.*, 2022, **1254**, 132422.

55 B. G. Youssif, A. M. Gouda, A. H. Moustafa, A. A. Abdelhamid, H. A. Gomaa, I. Kamal and A. A. Marzouk, *J. Mol. Struct.*, 2022, **1253**, 132218.

56 M. T.-E. Maghraby, T. Mazyad Almutairi, S. Bräse, O. I. A. Salem, B. G. M. Youssif and M. M. Sheha, *Molecules*, 2023, **28**, 7092.

57 M. F. Abo-Ashour, W. M. Eldehna, R. F. George, M. M. Abdel-Aziz, M. M. Elaasser, N. M. A. Gawad, A. Gupta, S. Bhakta and S. M. Abou-Seri, *Eur. J. Med. Chem.*, 2018, **160**, 49–60.

58 H. Hashem, A. Hassan, W. M. Abdelmagid, A. G. Habib, M. A. Abdel-Aal, A. M. Elshamsy, A. El Zawily, I. T. Radwan, S. Bräse and A. S. Abdel-Samea, *Pharmaceuticals*, 2024, **17**, 1154.

59 A. A. Ahmed, A. F. Mohammed, Z. M. Almarhoon, S. Bräse and B. G. Youssif, *Front. Chem.*, 2025, **12**, 1541846.

60 S. Wei, C. Han, S. Mo, H. Huang and X. Luo, *Apoptosis*, 2025, **30**, 401–421.

61 M. Mosadegh, N. Noori Goodarzi and Y. Erfani, *Cancer Invest.*, 2025, 1–26.

62 V. Jakhmola, T. Parashar, P. Ghildiyal, A. Ansori, R. K. Sharma, N. R. Rao, K. Kalra, N. Singh, N. Nainwal and R. K. Singh, *Pharmacogn. J.*, 2022, **14**, 190–205.



63 J. Eberhardt, D. Santos-Martins, A. F. Tillack and S. Forli, *J. Chem. Inf. Model.*, 2021, **61**, 3891–3898.

64 T. N. H. Pham, T. H. Nguyen, N. M. Tam, T. Y. Vu, N. T. Pham, N. T. Huy, B. K. Mai, N. T. Tung, M. Q. Pham and V. V. Vu, *J. Comput. Chem.*, 2022, **43**, 160–169.

65 S. Son, A. Elkamhawy, A. R. Gul, A. A. Al-Karmalawy, R. Alnajjar, A. Abdeen, S. F. Ibrahim, S. O. Alshammari, Q. A. Alshammari and W. J. Choi, *J. Enzyme Inhib. Med. Chem.*, 2023, **38**, 2202358.

66 J. Dong and X. Hao, *Front. Pharmacol.*, 2025, **16**, 1534707.

67 B. Bakchi, A. D. Krishna, E. Sreecharan, V. B. J. Ganesh, M. Niharika, S. Maharshi, S. B. Puttagunta, D. K. Sigalapalli, R. R. Bhandare and A. B. Shaik, *J. Mol. Struct.*, 2022, **1259**, 132712.

68 P. O. Lohohola, B. M. Mbala, S.-M. N. Bambi, D. T. Mawete, A. Matondo and J. G. M. Mvondo, *Int. J. Trop. Dis. Health*, 2021, **42**, 1–12.

